ERDC/GSL TR-23-19

Geotechnical and Structures Laboratory

US Army Corps
of Engineers®
Engineer Research and
Development Center

ERDC
ENGINEER RESEARCH & DEVELOPMENT CENTER

Graphene Applications for Military Engineering

Graphene in Cementitious Materials

Mine G. Ucak-Astarlioglu, Jedadiah F. Burroughs, Charles A. Weiss Jr., Kyle L. Klaus, Stephen L. Murrell, Samuel L. Craig, Jameson D. Shannon, Robert D. Moser, Kevin M. Wyss, and James M. Tour

December 2023

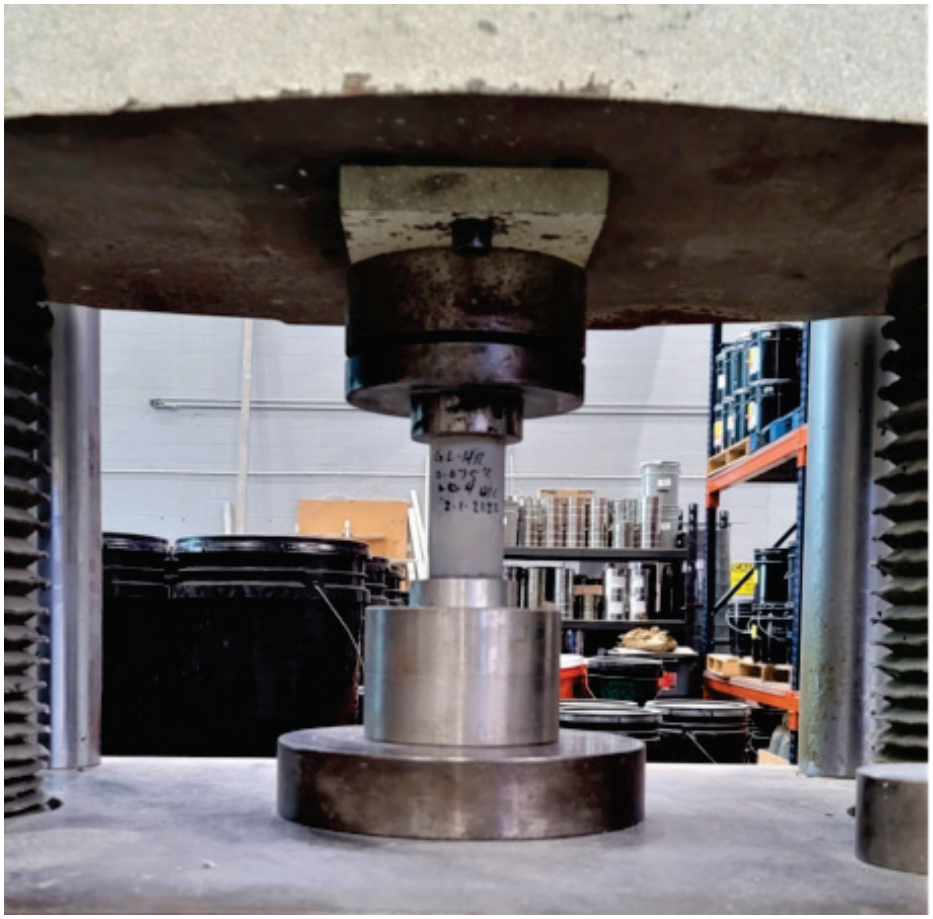

The US Army Engineer Research and Development Center (ERDC) solves the nation's toughest engineering and environmental challenges. ERDC develops innovative solutions in civil and military engineering, geospatial sciences, water resources, and environmental sciences for the Army, the Department of Defense, civilian agencies, and our nation's public good. Find out more at www.erdc.usace.army.mil.

To search for other technical reports published by ERDC, visit the ERDC online library at https://erdclibrary.on.worldcat.org/discovery.

ERDC/GSL TR-23-19
December 2023

Graphene in Cementitious Materials

Mine G. Ucak-Astarlioglu, Jedadiah F. Burroughs, Charles A. Weiss Jr., Kyle L. Klaus, Stephen L. Murrell, Samuel L. Craig, Jameson D. Shannon, and Robert D. Moser

US Army Engineer Research and Development Center (ERDC)
Geotechnical and Structures Laboratory (GSL)
3909 Halls Ferry Road
Vicksburg, MS 39180-6199

Kevin M. Wyss and James M. Tour

Rice University
NanoCarbon Center, MS-222
6100 Main St.
Houston, TX 77005

Final report

Prepared for Office of the Assistant Secretary of the Army for Acquisition, Logistics, and Technology (ASA[ALT])
Headquarters, US Army Corps of Engineers
441 G St. NW
Washington, DC 20314-1000

Under Project No. 505343, “Graphene Research”; Task No. BO340; Program Element No. 0603119A

Abstract

This project aims to determine the influence of laboratory-generated graphene (LGG) and commercial-grade graphene (CGG) on the chemical structure and compressive strength of graphene-cement mixtures. Determining the graphene-cement structure/processing/property relationships provides the most useful information for attaining the highest compressive strength. Graphene dose and particle size, speed of mixing, and dispersant agent were found to have important roles in graphene dispersion by affecting the adhesion forces between calcium silicate hydrate (CSH) gels and graphene surfaces that result in the enhanced strength of cement-graphene mixtures.

X-ray diffraction (XRD), Raman, and scanning electron microscope (SEM) analyses were used to determine chemical microstructure, and compression testing for mechanical properties characterization, respectively. Based on observed results both LGG and CGG graphene cement mixtures showed an increase in the compressive strength over 7-, 14-, and 28-day age curing periods. Preliminary dispersion studies were performed to determine the most effective surfactant for graphene dispersion.

Future studies will continue to research graphene—cement mortar and graphene—concrete composites using the most feasible graphene materials. These studies will prove invaluable for military programs, warfighter support, climate change, and civil works.

Contents

Abstract ii

Figures and Tables iv

Preface vii

1 Introduction 1

1.1 Background 1
1.2 Objectives 2
1.3 Approach 2

2 Experimental Approach 4

2.1 Selection of Graphene Material and Dispersant 4
2.2 Preparation of Graphene Dispersion in Water 5
2.2.1 Graphene Dispersion 5
2.2.2 Stabilized Aqueous Solution 7
2.3 Preparation of Graphene-Cement Mixtures 8
2.4 Cube and Cylinder Preparation for Curing Process 11
2.5 Mechanical Testing—Unconfined Compressive Strength Test 12
2.6 Chemical and Microstructure Analyses 12
2.6.1 X-Ray Photoelectron Spectroscopy (XPS) Analyses 12
2.6.2 Raman Analyses 13
2.6.3 Powder X-ray Diffraction (XRD) 13
2.6.4 Fourier-Transform Infrared Spectroscopy (FTIR) Analysis 13
2.6.5 Scanning Electron Microscopy (SEM)/Energy-Dispersive X-Ray Spectroscopy (EDS) Analyses 13
2.7 Mechanical Tests Methods and Results 14
2.8 Chemical and Microstructure Tests and Results 21

3 Discussion on Test Results of Laboratory-Generated Graphene (LGG) and Commercial-Grade Graphene (CGG) in Cementitious Materials 41

4 Conclusions and Recommendations 43

4.1 Conclusions 43
4.2 Recommendations 45

References 46

Appendix A: Graphene-Related Materials (GRM) Specifications 47

Appendix B: SEM/EDS Analyses 49

Abbreviations 53

Report Documentation Page

Figures and Tables

Figures

Figure 1. Dispersion of BW (Barite World) and TG (Turbo graphene) in water using MasterGlenium. 5
Figure 2. Dispersion of BW in water in the presence of ADVA® and MasterGlenium 7920. 6
Figure 3. Graphene interaction with dispersant. 6
Figure 4. High-shear-rate mixer. 7
Figure 5. Hobart mixer. 10
Figure 6. Graphene-cement mixture prepared in Hobart mixer bowl with dispersant. 10
Figure 7. 0.3% weight for weight (w/w) graphene in commercial-grade graphene (CGG)-cement mixtures in steel mold. 11
Figure 8. 0.3% (w/w) graphene in CGG-cement mixtures in plastic cylinders. 12
Figure 9. Before the application of load to 0.02% (w/w) laboratory-generated graphene (LGG)-cement paste. 14
Figure 10. After the application of load to 0.02% (w/w) LGG-cement paste. 15
Figure 11. Average compressive strength of LGG-based cement pastes at 14 and 28 days. 16
Figure 12. Normalized average compressive strength of LGG-based graphite-cement pastes at 14 and 28 days. 16
Figure 13. Maximum compressive strength of LGG-based graphite-cement pastes at 14 and 28 days. 17
Figure 14. Normalized maximum compressive strength of LGG-based graphite-cement pastes at 14 and 28 days. 17
Figure 15. Average compressive strength of CGG-based graphene-cement pastes at 7, 14, and 28 days. 19
Figure 16. Normalized average compressive strength of CGG-based graphite-cement pastes at 14 and 28 days. 19
Figure 17. LGG-based cement cubes obtained with 0.02% (w/w) to 0.62% (w/w) graphene percentages. 20
Figure 18. LGG-based cement cubes with 0.05% (w/w) graphene percentage. 21
Figure 19. LGG-based cement cubes with 2.08% (w/w) graphene percentage. 21
Figure 20. X-ray diffraction (XRD) of the white side of a LGG-based cement cube obtained from 0.05% graphene percentage. 22
Figure 21. XRD—chemical composition of the white side of 0.05% graphene in a LGG-based cement cube. 23
Figure 22. Scanning Electron Microscopy (SEM) analysis of 0.05% graphene in a LGG-based cement cube at 970x and 3,600x magnification. 23
Figure 23. Microstructure investigation of 0.3% CGG-based cement paste regions by SEM/Energy-Dispersive X-Ray Spectroscopy (EDS). 24

Figure 24. Dark gray (*region 1*) EDS—0.3% CGG-based cement paste. 25
Figure 25. Light gray (*region 2*) EDS of 0.3% CGG-based cement paste. 25
Figure 26. Black (*region 3*) EDS of 0.3% CGG-based cement paste. 25
Figure 27. Polished graphene-cement samples for SEM/EDS. 27
Figure 28. CGG-based cement paste, 0.3% graphene, at 77× magnification. 28
Figure 29. CGG-based cement paste, 0.3% graphene, at 2,000× magnification. 28
Figure 30. CGG-based cement paste, 0.9% graphene, at 77× magnification. 29
Figure 31. CGG-based cement paste, 0.9% graphene, at 2,000× magnification. 29
Figure 32. Reference cement paste without graphene at 77× magnification. 30
Figure 33. Reference cement paste without graphene at 1,000× magnification. 30
Figure 34. Reference cement paste without graphene at 2,000× magnification. 31
Figure 35. High shear rate mixed CGG-based cement paste, 0.3% graphene, no dispersant, at 77× magnification. 32
Figure 36. High shear rate mixed CGG-based cement paste, 0.3% graphene, no dispersant, at 2,000× magnification. 32
Figure 37. SEM/EDS image of high shear rate mixed CGG-based cement paste, 0.3% graphene, with dispersant, at 498× magnification. 33
Figure 38. EDS chemical microstructure analysis of high shear rate mixed CGG-based cement paste, 0.3% graphene, with dispersant, at 498× magnification. 34
Figure 39. EDS chemical microstructure analysis for carbon in CGG-based cement paste with 0.3% graphene. 34
Figure 40. EDS elemental composition analysis map for CGG-based cement paste with 0.3% graphene. 35
Figure 41. Powder XRD of reference paste and 0.3% and 0.9% graphene in CGG-based cement pastes. 36
Figure 42. Powder XRD of reference paste and 0.3% CGG-based cement pastes with and without dispersant in the presence of high-shear-rate mixing. 37
Figure 43. Raman spectra of reference paste, and 0.3% and 0.9% graphene in CGG-based cement pastes. 38
Figure 44. XPS spectra of xGnP® grade C-750 and BF-103. 39
Figure 45. FTIR spectra of reference paste, and 0.3% and 0.9% graphene in CGG-based cement pastes. 40
Figure A-1. xGnP® grade C-750. 47
Figure A-2. Barite World Graphite® BF-103. 48
Figure B-1. Color codes of elements in the map. 49
Figure B-2. EDS map of oxygen. 50
Figure B-3. EDS map of aluminum. 50
Figure B-4. EDS map of silicon. 51
Figure B-5. EDS map of iron. 51
Figure B-6. EDS map of calcium. 52
Figure B-7. EDS map of magnesium. 52

Tables

Table 1. Mixture proportions for graphene-cement paste made from LGG. 8
Table 2. Mixture proportions for graphene-cement paste made from CGG. 9
Table 3. XPS survey spectra—% atomic content summary. 22
Table 4. Elemental composition at different spots of 0.3% CGG-based cement paste. 26
Table 5. EDS Elemental composition for CGG-based cement paste with 0.3% graphene. 35

Preface

This study was conducted for the Office of the Assistant Secretary of the Army for Acquisition, Logistics, and Technology (ASA[ALT]) under Project No.505343, "Graphene Research"; Task No. BO340; and Program Element No. 0603119A. The technical monitor was Ms. Pamela G. Kinnebrew.

The work was performed by the Concrete and Materials Branch (GMC) of the Engineering Systems and Materials Division (GM), US Army Engineer Research and Development Center, Geotechnical and Structures Laboratory (ERDC-GSL). At the time of publication, Dr. Jameson Shannon was chief, GMC; Mr. Justin S. Strickler was chief, GM; and Ms. Pamela G. Kinnebrew was the technical director for Force Protection. The deputy director of the ERDC-GSL was Mr. Charles W. Ertle II, and the director was Mr. Bartley P. Durst.

The authors would like to acknowledge Dr. Robert Moser, Mr. Brian Green, and Mr. Brad Songer for invaluable discussions on cementitious materials; Dr. Travis Thornell for discussions on dispersion; and Mr. Erik Alberts for discussions on Scanning Electron Microscopy (SEM) images, respectively.

COL Christian Patterson was the commander of ERDC, and Dr. David W. Pittman was the director.

1 Introduction

Novel cementitious materials are always in demand for military survivability and force protection applications as well as for tackling climate change effects due in part to CO_2 emissions from portland cement manufacturing processes. Innovative ways to prepare high-strength, high-durability, and low-permeability cementitious materials produced with reduced (or zero) CO_2 emissions is a goal of many international material and concrete organizations.

1.1 Background

The US Army Engineer Research and Development Center (ERDC) has a history of developing high-strength concrete mixtures and has the research expertise, capabilities, and facilities to synthesize and characterize novel cementitious materials.

Following Feynman's vision, "the essence of nanotechnology is the ability to work at the molecular level, atom-by-atom control, to create large structures with fundamentally new molecular organization" (Drexler 2004), researchers would like to interpret, control, and regulate structural changes of graphene-cementitious materials at every level.

Portland cement, the building block of concrete, goes through a hydration reaction when it reacts with water due to its chemical constituents: calcium silicates, aluminates, and aluminoferrite. In this reaction, it changes its form from powder to fibrous crystals (Lea 1970). The growth and interlocking of these fibrous crystals create a matrix that gives rise to the material properties of concrete. To make one form of novel cementitious material, graphene, a 2-D material, is introduced into the cement. Through graphene's interaction with portland cement, its special chemical and physical properties are exploited, and resulting internal matrix is enhanced. Graphene owes its special properties to its sp^2 hybridized carbon atoms that form a covalent bond, and each carbon atom is connected to three other carbon atoms in its crystal lattice. Carbon atoms in graphene have a unique hexagonal arrangement that facilitate free mobility of electrons across the layers making this 2-D material carry electrical charge or heat very effectively. This property gives graphene special mechanical, chemical, thermal, and electrical properties (Novoselov et al. 2004).

In this project, team members designed a graphene-cement preparation method that took advantage of the ERDC's laboratory and equipment modernization efforts. Experimentally, graphene-cement mixtures were prepared using graphene sourced from two different ways: first, based on the exfoliation of graphite into graphene that produced a product called laboratory-generated graphene (LGG), and second, using a commercial-grade graphene (CGG). Graphene-cement mixtures were then analyzed based on chemical, mechanical, and microstructure properties, and the results were compared to reference cement pastes without graphene.

1.2 Objectives

The primary objectives of this research were to prepare feasible graphene-cement mixtures and to characterize their mechanical, chemical, and microstructure properties.

Novel functionalities in cementitious materials can prevent the formation of chemical and mechanical defects and attain stronger cementitious materials. The graphene-cementitious materials developed in this research are targeted for use in military applications (i.e., for construction of resilient structures protecting against natural and manmade disasters while reducing the effects of global warming attributable to cement manufacturing).

1.3 Approach

In the first method, researchers exfoliated graphene from graphite to obtain LGG and, in the second method, used the purchased CGG "as is" in the preparation of practical graphene-cement mixtures. Then, team members characterized the properties of these materials by conducting chemical, mechanical, and microstructure analyses. Based on the results obtained, exfoliation of graphene proved to be a viable technique in graphene synthesis, and both methods showed feasible resulting in significant mechanical performance when placed in portland cement.

This research was divided into six major steps: the first was the selection of the graphite material and the dispersant; the second was synthesis and dispersion of graphene in water; third was the preparation of graphene-cement mixture; fourth was the curing process in a fog room; the fifth step was the compressive strength test analyses of graphene-cement mixtures; and the sixth step was chemical and microstructural analyses.

The performance of LGG-based cement mixture was compared to CGG-based cement mixture. In addition, both LGG- and CGG-based mixtures were compared to their reference cement pastes without graphene.

2 Experimental Approach

2.1 Selection of Graphene Material and Dispersant

Two types of graphene-related materials (GRM), graphite and graphene, were used in the preparation of graphene-cement mixtures. Cost, ease of dispersion, and mechanical performance were used as the selection criteria in the determination of the GRM used in this study. Results from these graphene-cement mixtures were compared to the reference cement mixtures that contain no graphene. Graphite grade BF-103 was purchased from Barite World (BW). Commercially available graphene nanoplatelet, xGnP® grade C-750, was purchased from XG-Sciences®. Graphite prices were found to be four times cheaper compared to graphene. These GRM have significantly different particle sizes as reported by their manufacturers: xGnP® C-750 less than 2 nm, and BF-103 4.6 to 27.2 μm* particle size range. Manufacturers' information on these GRM can be found in Appendix A. GRM surface areas were determined at an ERDC Environmental Laboratory facility using an Autosorb BET Instrument. Based on that, BF-103 was found to have a 1 m^2/g surface area, whereas xGnP® C-750 has 750 m^2/g. The differences in GRM particle sizes and surface areas may significantly affect the end result of microstructural and mechanical properties of graphene-cement mixtures (Ho et al. 2020).

To produce LGG, an exfoliation method was used to convert graphite into graphene through high-shear-rate mixing. Dispersant MasterGlenium 7920 was obtained from Master Builders Solutions, and ADVA®198 from GCP Applied Technologies. Zeta potential analyses as well as visual inspection of aqueous graphene dispersion over time were conducted to determine the best dispersant.

* For a full list of the spelled-out forms of the units of measure used in this document, please refer to *US Government Publishing Office Style Manual*, 31st ed. (Washington, DC: US Government Publishing Office, 2016), 248–252, https://www.govinfo.gov/content/pkg/GPO-STYLEMANUAL-2016/pdf/GPO-STYLEMANUAL-2016.pdf.

2.2 Preparation of Graphene Dispersion in Water

2.2.1 Graphene Dispersion

Dispersion of the GRM was found in the literature to be the most common obstacle in the cementitious environment (Gronchi et al. 2018). In the preparation of graphene pastes, dispersion and agglomeration prevention was found to be critically dependent on the dispersant type and amount, and mixing speed. Agglomeration causes many layers of graphene to come together. These multi layers are held together by weak van der Waals forces and displacement of layers reduces the strength of graphene-cement mixtures (Dimov et al. 2018). Making a good dispersion will help to understand the true enhancement abilities of GRM materials in applications. Figure 1 shows dispersion study of BW graphene, and Turbo graphene (TG), synthesized at Rice University, in MasterGlenium 7920 dispersant. Figure 2 shows the dispersion comparison for BW in two different dispersants, ADVA and MasterGlenium, and in water. Figure 3 shows the interaction of dispersant polycarboxylate molecule with stacks of graphene. The backbone of the dispersant molecule absorbs on the surface of graphene while its side chains with negative charges repel graphene particles from each other through electrostatic repulsion.

To prepare aqueous graphene dispersion solutions, ADVA and MasterGlenium dispersants or high-range water-reducing admixtures (HRWRA) were tested. Mixing dispersant and water in a vial, graphene was added, and the solution was sonicated using a QSonica sonicator for 2 min. Sonicator creates shock waves to provide high enough energy to break the inter-layer van der Waals bonds in graphite (Hernandez et al. 2008).

Figure 1. Dispersion of BW (Barite World) and TG (Turbo graphene) in water using MasterGlenium.

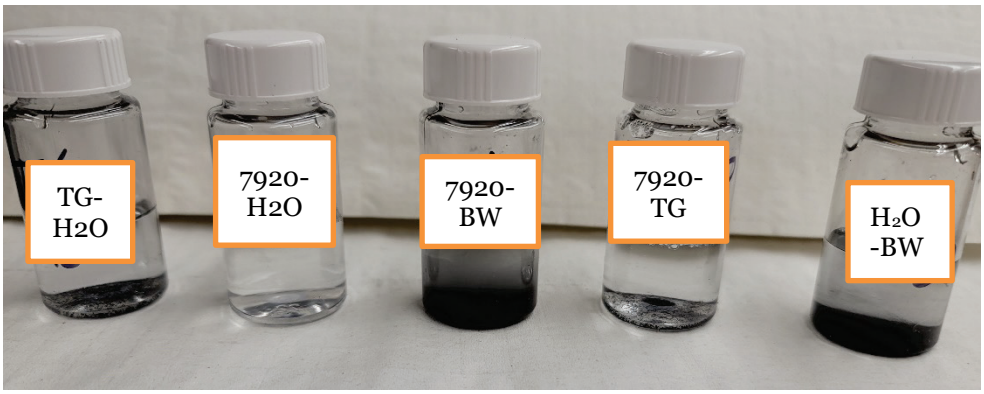

Figure 2. Dispersion of BW in water in the presence of ADVA® and MasterGlenium 7920.

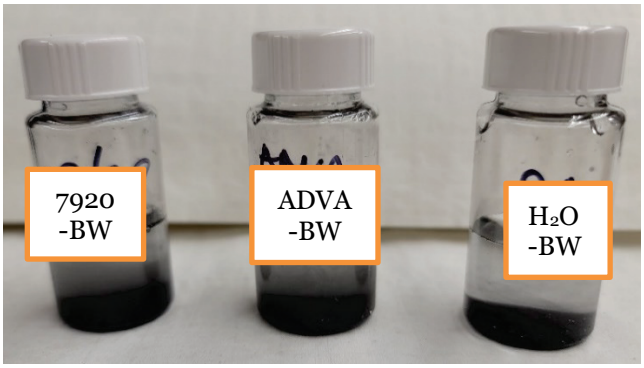

Figure 3. Graphene interaction with dispersant.

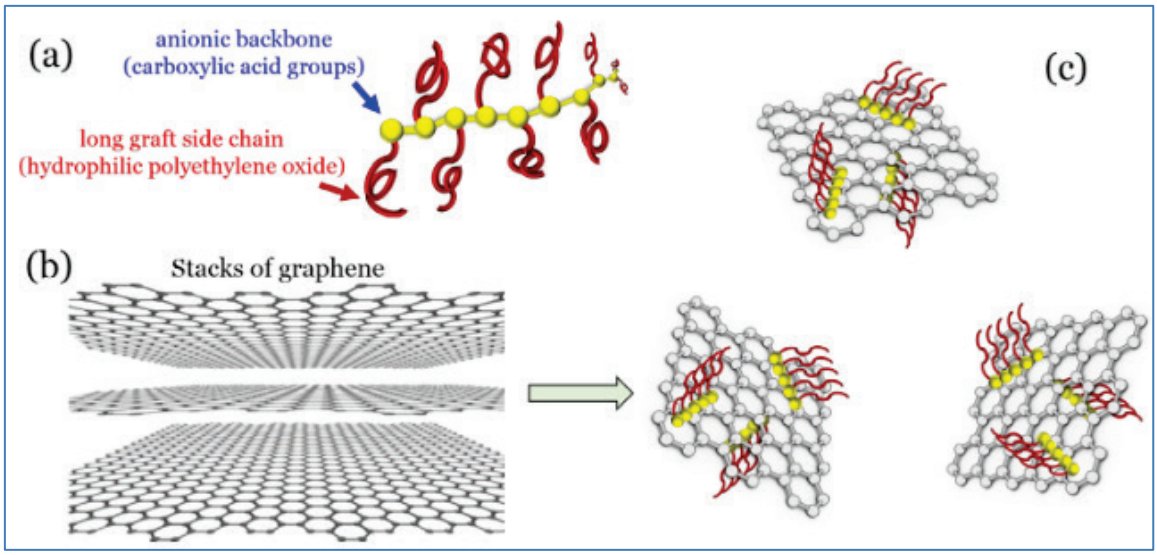

(a) Dispersant, (b) stacks of graphene, and (c) interaction of dispersant and graphene (Du and Pang 2018).

Sonicated samples were tested using a Malvern Zetasizer instrument. Zeta potential reveals the long-term stability of graphene dispersion matrices by determining the magnitude of the interaction based on the surface charge characteristics of graphene particles. Zeta potential measurements were conducted in the presence and absence of dispersants. The zeta potential values of the dispersions in the presence of MasterGlenium 7920 HRWRA were above |30| mV indicating a good stability.

For use in the graphene-cement mixture preparations, graphene was first placed in a stabilized aqueous dispersant solution and sonicated. Following that a Waring Commercial MX1300XTX 3.5-horsepower high-shear-rate mixer was used at the rate of 5,000 rpm for 20 min as

shown in Figure 4. High shear exfoliation uses a shear force to separate the graphene sheets (Xu et al. 2018).

Figure 4. High-shear-rate mixer.

Besides different dispersants and graphene materials, the effect of the pH on the aqueous media and presence of pore solution were also investigated in the media where graphene dispersion took place. Pore solution was prepared by placing 1 N NaOH (17.94 g), 1 N KOH (5.24 g), and $Ca(OH)_2$ (2.4 g) in 1 L of distilled water and stirred using a stirring plate. Graphene material and dispersant were placed in this aqueous media for preliminary observation of dispersion.

2.2.2 Stabilized Aqueous Solution

To obtain a stabilized aqueous solution, water and a predetermined optimum dose of dispersant were stirred magnetically for complete dispersant solubilization.

2.3 Preparation of Graphene-Cement Mixtures

Table 1 shows the graphene-cement mixture proportions, using exfoliated BW graphite into graphene, in the preparation of LGG-based cement mixtures. The mixtures used Type I/II cement portland cement meeting the requirements of ASTM C150/C150M-19 (2019) that was sourced from Holcim USA's St. Genevieve, Missouri, kiln. MasterGlenium 7920 HRWRA was used as the dispersant at a constant dosage that was based on the amount needed for 1 µL/mg at the highest 2.08% graphite dosage. The MasterGlenium 7920 HRWRA amount for these mixtures was 2.26% by mass of cement. Using tap water, the water-to-cement ratio (w/c) was kept constant at w/c = 0.25.

Each batch of graphene-cement mixture produced nine 2 in. cubes and three 1 in. × 1 in. × 12 in. long prisms. The method prescribed in ASTM C1856/C1856M-17 (2017) flow test was applied by filling a conical mold in one lift, removing the mold and allowing the mixture to spread for 2 min, then measuring 2 diam, and taking the average.

Table 1. Mixture proportions for graphene-cement paste made from LGG.

Graphene %	m_{HRWR} (lb)	w/c	m_{cement} (lb)	$m_{graphite}$ (lb)	$m_{water,mix}$ (lb)
0.00 (Reference)	0.69	0.25	30.90	0.00	7.72
0.02	0.69	0.25	30.90	0.01	7.72
0.05	0.69	0.25	30.89	0.02	7.72
0.21	0.69	0.25	30.85	0.06	7.71
0.62	0.69	0.25	30.75	0.20	7.69
2.08	0.69	0.25	30.41	0.63	7.60

Table 2 shows the graphene-cement mixture proportions, using XG-Sciences xGnP®C-750 graphene, in CGG-based cement paste preparation. For the CGG study, the dispersant dosage varied based on the graphene amount because of 1.84 factor of graphene weight for weight (w/w). Graphene % shows the graphene-to-cement ration by weight. Using tap water, w/c = 0.40 was held constant. Nine 2 in. cubes and three 1 in. × 1 in. × 12 in. long prisms were cast from each mixture. The methods prescribed in ASTM C1856/C1856M-17 (2017) were used to measure the flow of the mixture by filling the conical mold in one lift, removing the mold, allowing the mixture to spread for 2 min, measuring 2 diam, and taking the average.

Table 2. Mixture proportions for graphene-cement paste made from CGG.

Graphene %	m_{HRWR} (lb)	w/c	m_{cement} (lb)	$m_{graphene}$ (lb)	$m_{water,mix}$ (lb)
0.00 (Reference)	0.00	0.40	7.57	0.00	3.03
0.3	0.01	0.40	7.55	0.02	3.01
0.6	0.02	0.40	7.53	0.05	3.00
0.9	0.04	0.40	7.52	0.07	2.98

- ASTM Type I/II cement and MasterGlenium 7920 HRWRA was used in all cement paste mixtures.
- For LGG, dispersion dosage used was based onto an amount needed for 1 µL/mg at 2.08% graphite dosage that was 2.26% w/w cement.
- For CGG, dispersant dosage was based onto the graphene amount used and determined as a 1.84 factor of graphene (w/w).
- Graphene % shows the graphene-to-cement ratio by weight.

Preparing Graphene-Cement Paste Using High-Shear-Rate Mixer with HRWRA

Stabilized aqueous graphene dispersant solution was placed into a Waring Commercial MX1300XTX 3.5-hp high-shear-rate mixer at the rate of 5,000 rpm for 20 minutes (Figure 4). This dispersed graphene solution was then mixed with the portland cement. A Hobart mixer (Figure 5) was used in the preparation of the graphene-cement pastes.

Figure 5. Hobart mixer.

The dispersed graphene solution was placed into the Hobart mixing bowl, and then the portland cement was added. After mixing at a slow speed of 140 ± 5 rpm for 60 sec, the mixer was stopped for 30 sec to scrape down the paste collected on the sides of the bowl, and mixing was continued at medium speed (285 ± 10 rpm) for 10 min. Figure 6 shows the graphene-paste prepared by Hobart mixer.

Figure 6. Graphene-cement mixture prepared in Hobart mixer bowl with dispersant.

Preparing Graphene-Cement Paste Using High Shear Rate Mixer without HRWRA

The impact of dispersant on the dispersion of graphene and on the performance of graphene-cement mixture were investigated. Graphene-cement mixtures were prepared using a high-shear-rate mixer without dispersant as described in Section 2.3.1.

2.4 Cube and Cylinder Preparation for Curing Process

The graphene-cement paste was cast into 2 in. diam × 4 in. tall plastic cylindrical molds and 2 in. cubical stainless-steel molds. External vibration was applied to cylinders and cubes. After casting, the paste that had been forced out onto the tops of the molds was smoothed with a trowel and left in moist for curing (fog room) until 7-, 14-, or 28-day age. Upon curing, unconfined compressive strength testing was conducted at room temperature. Figures 7 and 8 show the fresh 0.3% (w/w) graphene in CGG-based cement mixtures before left out for curing in steel mold and plastic cylinders.

Figure 7. 0.3% weight for weight (w/w) graphene in commercial-grade graphene (CGG)-cement mixtures in steel mold.

Figure 8. 0.3% (w/w) graphene in CGG-cement mixtures in plastic cylinders.

2.5 Mechanical Testing—Unconfined Compressive Strength Test

The American Society for Testing and Materials, ASTM C39/C39M-21 (*ASTM C39/C39M-21 Standard Test Method for Compressive Strength of Cylindrical Concrete Specimens [2021a]*) was used in testing the cylinders. To test the cubes, ASTM C109/C109M-21 (2021b) was used. Mechanical tests were performed immediately after taking the samples out of the fog room.

2.6 Chemical and Microstructure Analyses

2.6.1 X-Ray Photoelectron Spectroscopy (XPS) Analyses

All X-ray photoelectron spectroscopy (XPS) data were collected using a PHI Quantera SXM Scanning X-Ray Microprobe with a base pressure of 5×10^{-9} torr. Survey spectra were recorded using 0.5-eV step sizes with a pass energy of 140 eV. Elemental spectra were recorded using 0.1 eV step sizes with a pass energy of 26 eV. Spectra were not corrected to 284.5 eV or Shirley baseline subtracted.

2.6.2 Raman Analyses

All Raman spectra were collected using a Renishaw inVia Raman microscope outfitted with a 5 mW, 532 nm laser using a 50x objective lens. High-resolution single Raman spectra were collected and used for Lorentzian peak fitting. Because cement has high amounts of background fluorescence, a MatLab script was used to subtract the background in processing the raw data.

2.6.3 Powder X-ray Diffraction (XRD)

All powder X-ray diffraction (XRD) patterns were collected using a Rigaku SmartLab II using zero background sample holders at a scan rate of 8 $^{o}2\theta$ /min and a 0.015 $^{o}2\theta$ step size.

2.6.4 Fourier-Transform Infrared Spectroscopy (FTIR) Analysis

All Fourier-Transform Infrared Spectroscopy (FTIR) spectra were collected using a Nicolet FTIR microscope with a liquid nitrogen-cooled detector. An attenuated total reflection (ATR) attachment was used to collect data from the surface of the cement composite samples. A background was collected before each sample was collected.

2.6.5 Scanning Electron Microscopy (SEM)/Energy-Dispersive X-Ray Spectroscopy (EDS) Analyses

Two different types of Scanning Electron Microscopy (SEM)/Energy-Dispersive X-Ray Spectroscopy (EDS) analyses were performed for preliminary and sophisticated data analyses. Sophisticated analysis has higher resolution than the preliminary SEM/EDS set up. For the sophisticated analyses, SEM was performed using a FEI Nova NanoSEM 630 under low vacuum at pressures of 0.1 to 0.5 mbar and an accelerating voltage of 15 kV. All images were taken using a backscattered electron detector or low voltage-high contrast detector (VCD). Imaging was performed in multiple locations on each sample to observe an accurate representation. EDS is used in conjunction with SEM imaging to perform chemical microanalysis of a specimen. EDS was performed using a Bruker Quan-tax AXS detector, which attached directly to the SEM. This analysis can focus data collection to a single point or the entire field of view. EDS mapping assigns colors to the area's constituents to aid in differentiation. The software can output collected data in many ways including atomic percentages, major oxides, or individual elements.

2.7 Mechanical Tests Methods and Results

Before and after pictures of an unconfined compressive strength test for the 0.0208% LGG cement mixture is shown in Figures 9 and 10, respectively. The same constant load rate was applied to all specimens during this research based onto the ASTM C109/C109M-21 standard for cube tests. The average of three test results were taken as the representative compressive strength.

Figure 9. Before the application of load to 0.02% (w/w) laboratory-generated graphene (LGG)-cement paste.

Figure 10. After the application of load to 0.02% (w/w) LGG-cement paste.

Figure 11 shows the average compressive strength for LGG-cement pastes after 14- and 28-day curing. Figure 12 shows strength versus curing duration, where $r_{strength}$ is the average compressive strength of the graphene-cement paste normalized as a percentage of the average compressive strength of the reference cement paste.

Figures 13 and 14 show the average compressive strength of LGG-based cement pastes at 14- and 28-day curing. Figure 14 shows $r_{strength,\ maximum}$ versus curing time, where $r_{strength,\ maximum}$ is the maximum compressive strength of the graphene-cement paste based on a normalized percentage of the maximum compressive strength of the reference cement paste.

Figure 11. Average compressive strength of LGG-based cement pastes at 14 and 28 days.

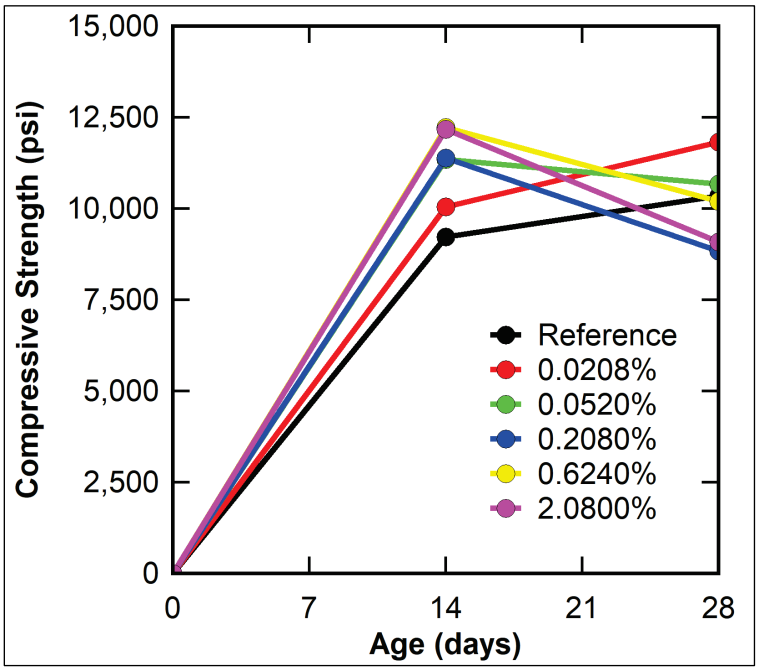

Figure 12. Normalized average compressive strength of LGG-based graphite-cement pastes at 14 and 28 days.

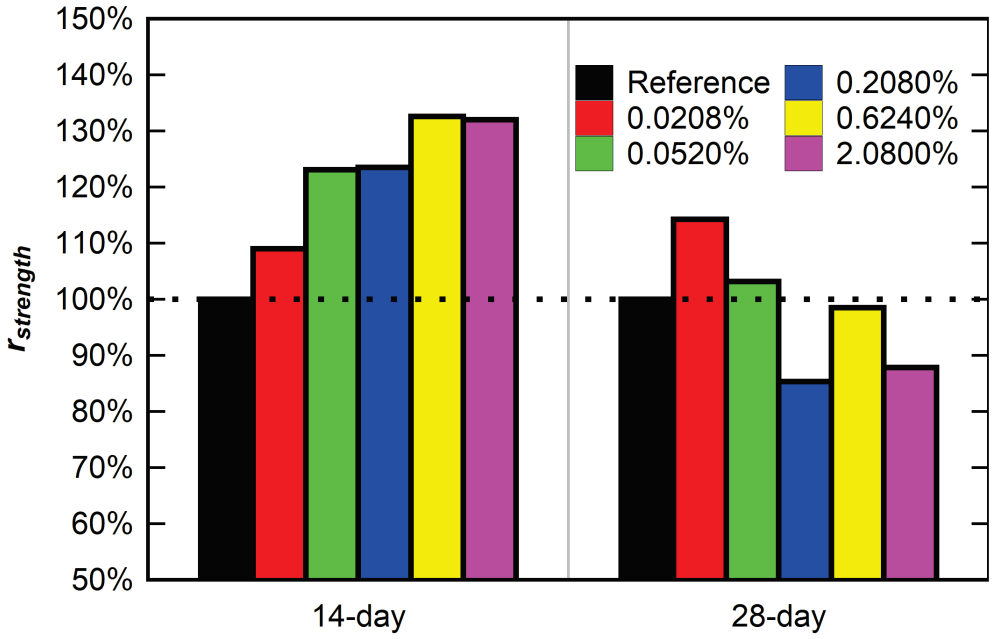

Figure 13. Maximum compressive strength of LGG-based graphite-cement pastes at 14 and 28 days.

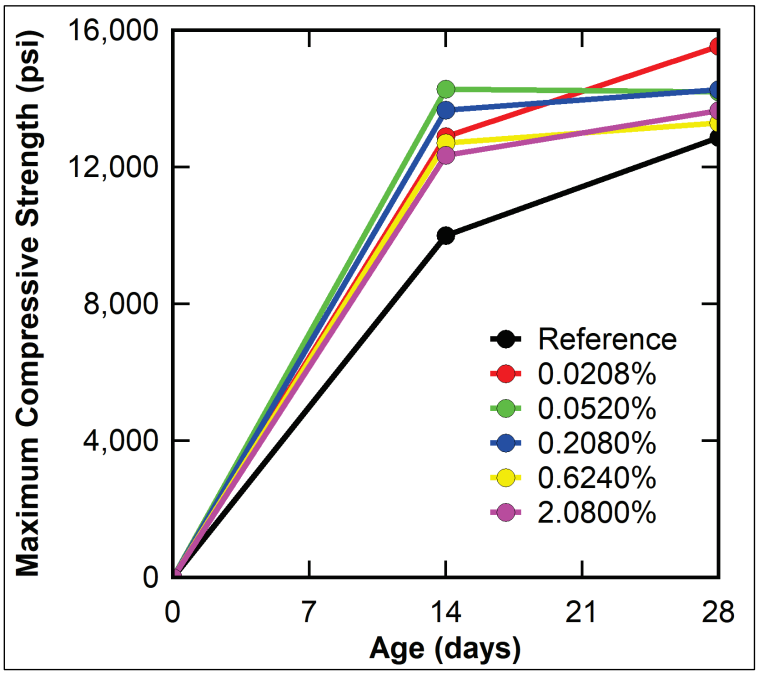

Figure 14. Normalized maximum compressive strength of LGG-based graphite-cement pastes at 14 and 28 days.

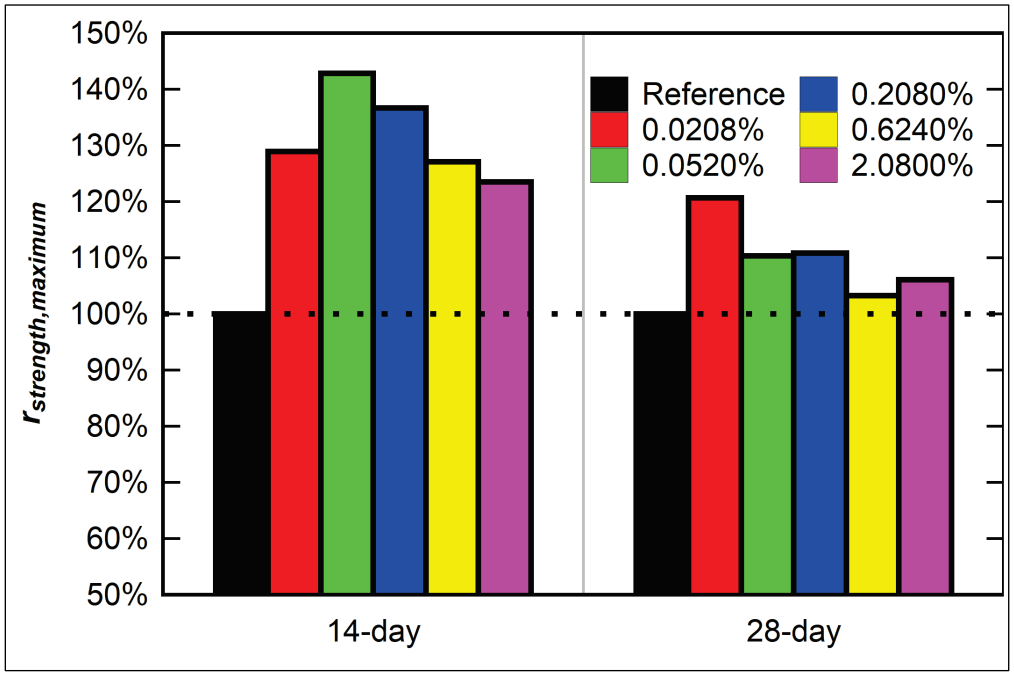

Figure 15 shows compressive strength versus curing time for graphene-cement paste prepared from CGG for 7-, 14-, and 28-day curing for averaged repetitions. Figure 16 shows $r_{strength}$ versus curing time, where

$r_{strength}$ is the average compressive strength of the graphene-cement paste normalized as a percentage of the average compressive strength of the reference cement paste.

Figures 11 and 15 indicate a significant increase in the average compressive strength for 7- and 14-day curing compared to the reference cement paste for both LGG- and CGG-based cement mixtures. Among all the graphene percentages considered, the lowest graphene loadings (0.05%, and 0.02%) presented the highest compressive strength increase relative to the other concentrations of LGG and CGG. However, at 28 days curing, the increase in compressive strength decreases for these highest percentages of graphene. On the other hand, the lowest graphene percentage (0.02%) of graphene-cement paste shows stabilization of increased compressive strength at 28 days. These observations are clearly supported by Figure 12, $r_{strength}$ is the average compressive strength of the graphene-cement paste normalized as a percentage of the average compressive strength of the reference cement paste.

Figure 15 indicates a general increase in the compressive strength for all graphene percentages at seven and 14 days as compared to the reference cement paste. It was observed that after 14 days, compressive strengths start to level off for almost all the graphene percentages except for the lowest percentage (0.3%). These trends can also be observed in Figure 16 where 0.3% graphene cement paste shows an increase in compressive strength from 7 to 28 days.

Figure 15. Average compressive strength of CGG-based graphene-cement pastes at 7, 14, and 28 days.

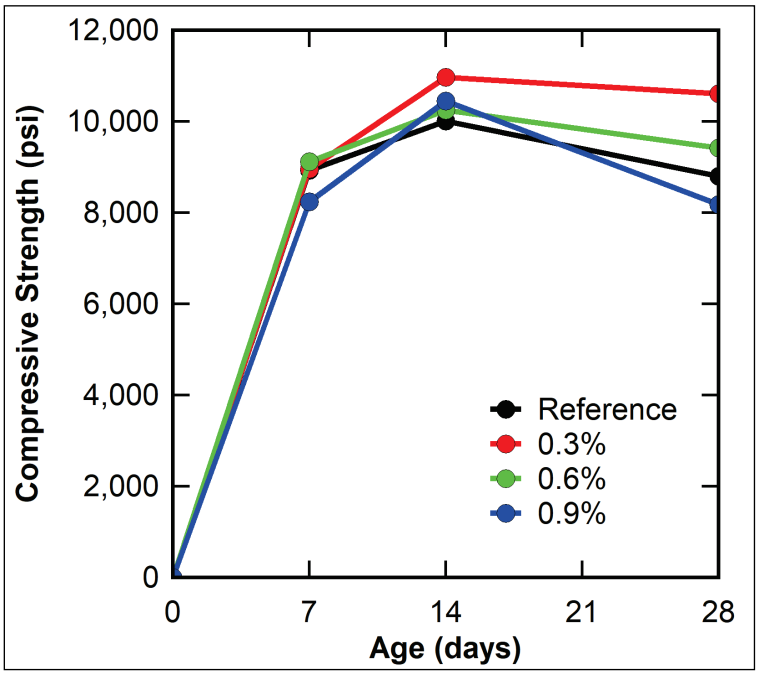

Figure 16. Normalized average compressive strength of CGG-based graphite-cement pastes at 14 and 28 days.

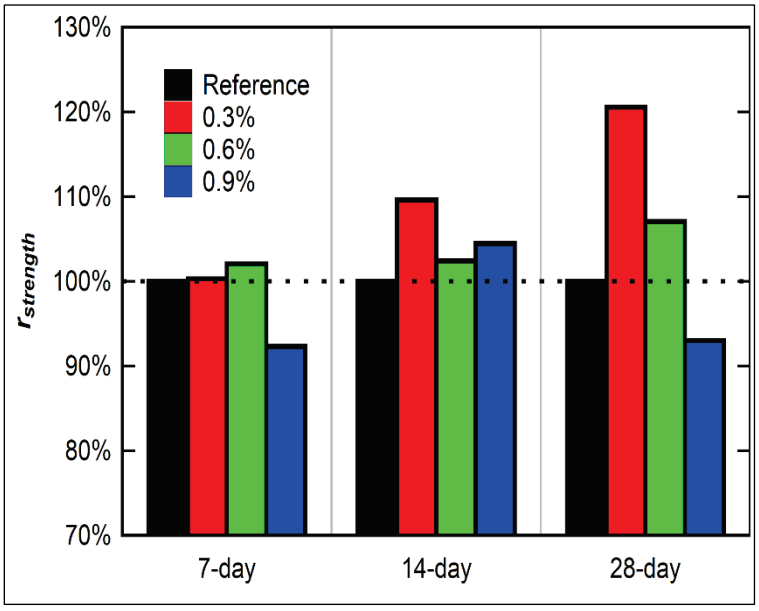

Figure 17 shows light-colored calcite deposits on the top faces of all LGG-based cement cubes. Visual investigation suggests that highest level of calcite forms at the lowest graphene percentages in LGG-based cement mixture cubes. This difference can be clearly observed in Figure 18 with 0.05% LGG and Figure 19 with 2.08% LGG graphene percentages.

Different sides of the cube need to be further analyzed to assess whether the white calcite formation may be due to contact with air and/ or possibly due to the moisture in the air in the fog room.

Figure 17. LGG-based cement cubes obtained with 0.02% (w/w) to 0.62% (w/w) graphene percentages.

Figure 18. LGG-based cement cubes with 0.05% (w/w) graphene percentage.

Figure 19. LGG-based cement cubes with 2.08% (w/w) graphene percentage.

2.8 Chemical and Microstructure Tests and Results

In the chemical investigation of graphene-cement paste; XPS, XRD, FTIR, and Raman spectroscopy; and for microstructure analyses SEM/EDS was used.

In the chemical analyses XPS was used as a tool to determine the atomic species and their atomic percentages in the starting graphene materials. Table 3 shows the summary of % atomic contents of graphite and the

graphene powders used in the preparation of graphene-cement mixtures based on the XPS survey spectra.

Table 3. XPS survey spectra—% atomic content summary.

Graphene Material	% Atomic Content						
	C	O	Si	N	Al	Cl	F
BA Graphite Powder	95.1	2.7	–	–	–	–	2.2
xGnP© C-750 Sciences Graphene Powder	93.8	6.2	–	–	–	–	–

XRD chromatography was employed to investigate the white calcite formation on the sides of the cubes. Figure 20 shows XRD of the white-calcite site of the graphene-cement cube with 0.05% LGG, and Figure 21 presents its chemical composition, respectively.

Figure 20. X-ray diffraction (XRD) of the white side of a LGG-based cement cube obtained from 0.05% graphene percentage.

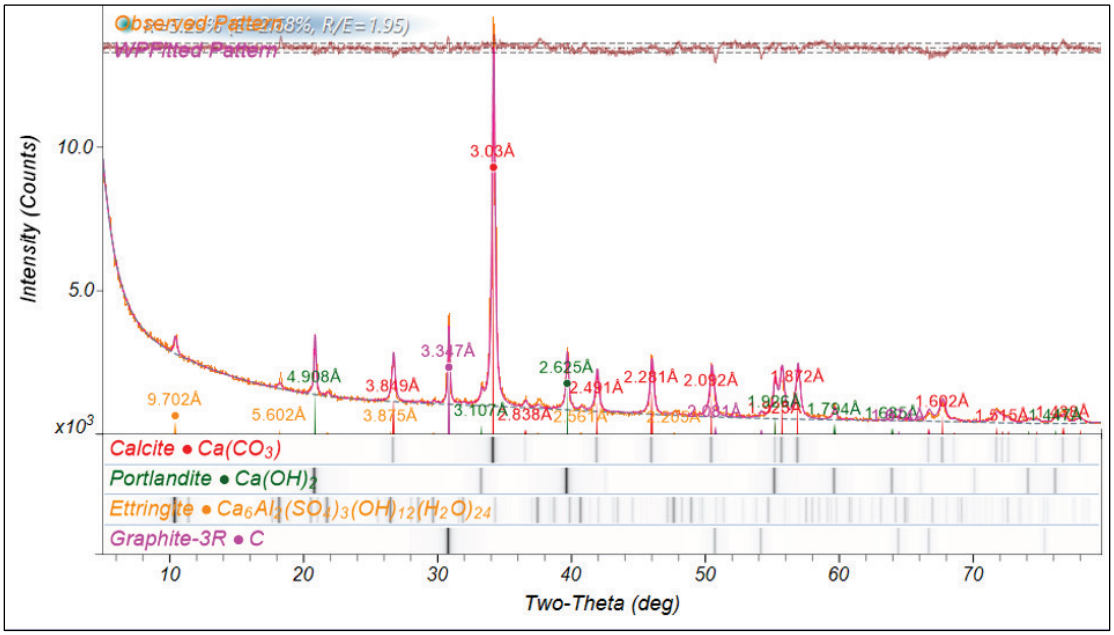

Figure 21. XRD—chemical composition of the white side of 0.05% graphene in a LGG-based cement cube.

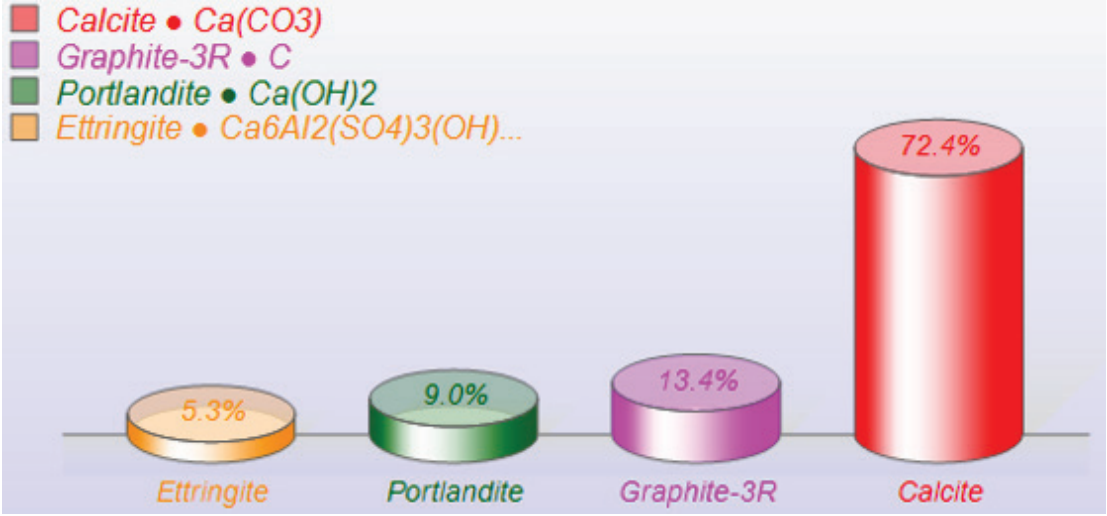

To further characterize the white calcite sites of the graphene-cement mixtures, SEM/EDS analyses were conducted with a benchtop SEM/EDS using nonpolished samples as presented in Figure 22. XRD analyses showed remaining hydration products as portlandite, ettringite, and graphite. As expected, the SEM/EDS analysis indicated that the white site has a layer of calcium oxide/hydroxide.

Figure 22. Scanning Electron Microscopy (SEM) analysis of 0.05% graphene in a LGG-based cement cube at 970x and 3,600x magnification.

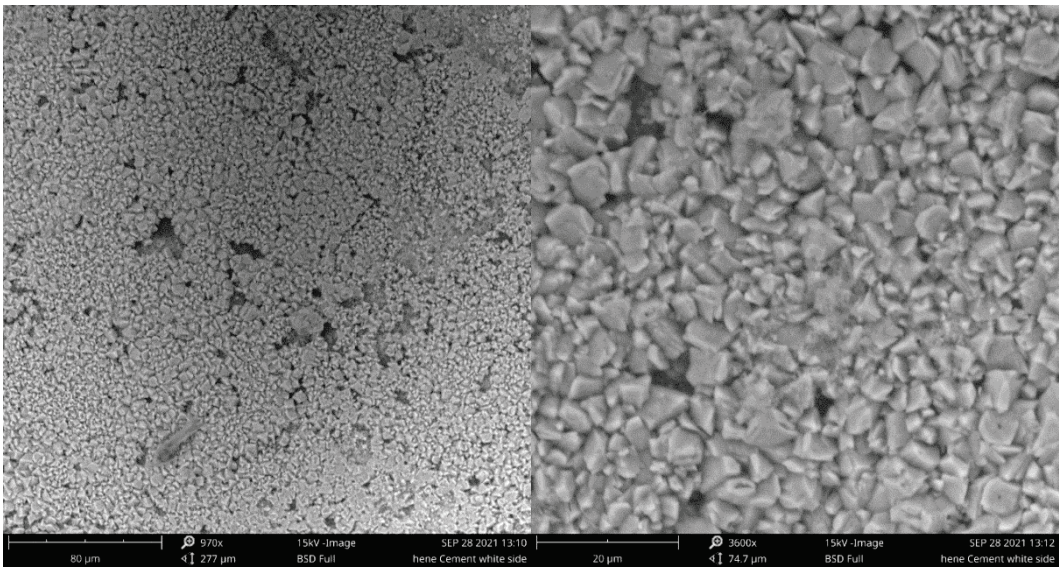

(a) 970x magnification (b) 3600x magnification

Figure 23 presents three different regions of 0.3% CGG-based cement paste by color. These regions, labeled as 1, 2, and 3, correspond to dark gray, light gray, and black zones, respectively. These regions were used to analyze the white calcite layer and the black layer underneath. The dark gray side is the hydrated cement, and light gray is the dehydrated cement sites.

Figure 23. Microstructure investigation of 0.3% CGG-based cement paste regions by SEM/Energy-Dispersive X-Ray Spectroscopy (EDS).

EDS elemental mapping confirmed the incorporation of calcite formation in the graphene-cement mixtures where sample contacted with air and/ or possibly moisture in the air in the fog room.

Figures 24, 25, and 26 show the EDS elemental analyses for these regions, and Table 4 presents the atomic concentration of elements in all the regions of the graphene-cement paste, respectively.

Figure 24. Dark gray (*region 1*) EDS—0.3% CGG-based cement paste.

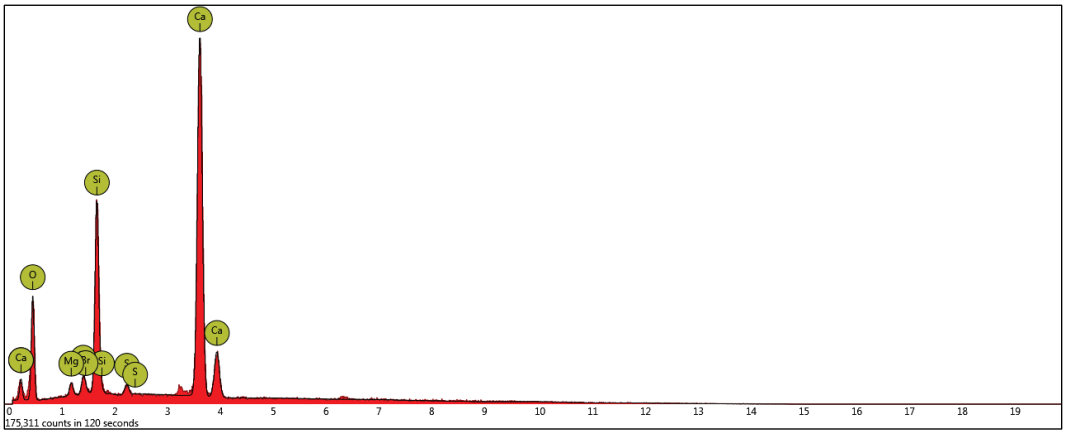

Figure 25. Light gray (*region 2*) EDS of 0.3% CGG-based cement paste.

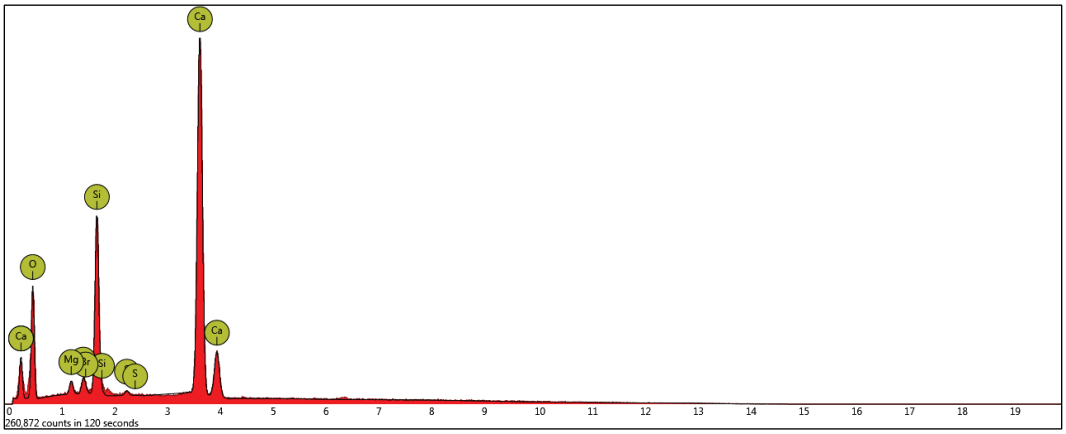

Figure 26. Black (*region 3*) EDS of 0.3% CGG-based cement paste.

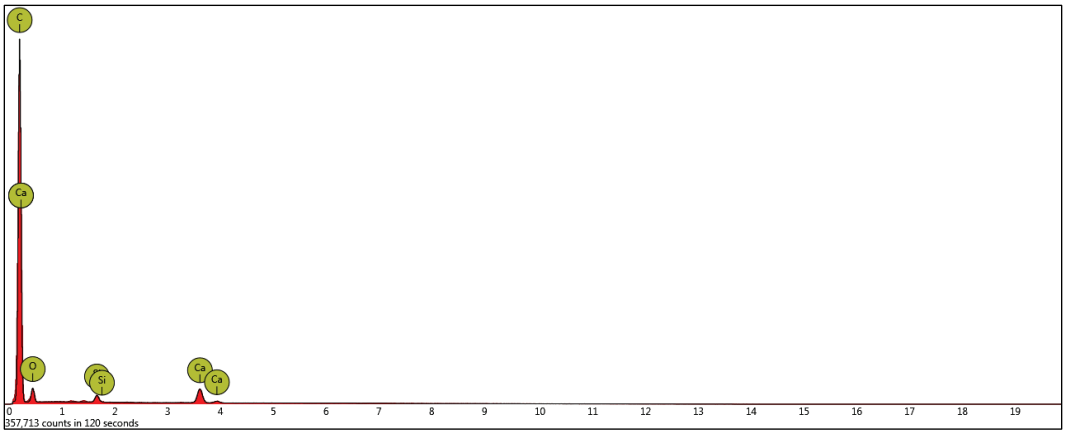

Table 4. Elemental composition at different spots of 0.3% CGG-based cement paste.

Elements	Dark Gray (Spot 1)		Light Gray (Spot 2)		Black (Spot 3)	
	AC%	AC%	AC%	WC%	AC%	WC%
Carbon (C)	—	—	—	—	59.56	48.58
Oxygen (O)	64.58	44.18	66.59	46.33	35.22	38.27
Calcium (Ca)	23.41	40.12	22.63	39.45	3.94	10.72
Silicon (Si)	9.46	11.36	8.59	10.49	1.28	2.44
Magnesium (Mg)	1.37	1.42	1.37	1.45	—	—
Aluminum (Al)	0.64	2.18-	0.55	1.93	—	—
Sulfur (S)	0.53	0.73	0.26	0.36	—	—

Atomic concentration: AC

Weight concentration: WC

SEM/EDS analyses were compared from a benchtop low-resolution SEM and a high-resolution SEM instrument. Based on the benchtop low-resolution SEM/EDS analyses of nonpolished samples, light and dark gray zones presented similar elemental composition (mostly calcium and silicon with trace amounts of other ions); this was the case even though they had different visual appearances. The black region presented predominantly carbon, with a 48.55% weight concentration, indicating graphene carbon. In this region, the oxygen identified, with 38.27 % weight concentration, was probably from the residual water, oxidized residue of graphene, from the sample chamber, or calcium and silicon from the surrounding region.

Following the preliminary low-resolution SEM/EDS analysis of nonpolished samples, high-resolution SEM/EDS analyses were performed on polished samples. These analyses were conducted to obtain more detailed images of graphene-cement paste microstructures. Figure 27 shows the polished graphene-cement samples used for SEM/EDS microstructure and chemical composition analysis.

Figure 27. Polished graphene-cement samples for SEM/EDS.

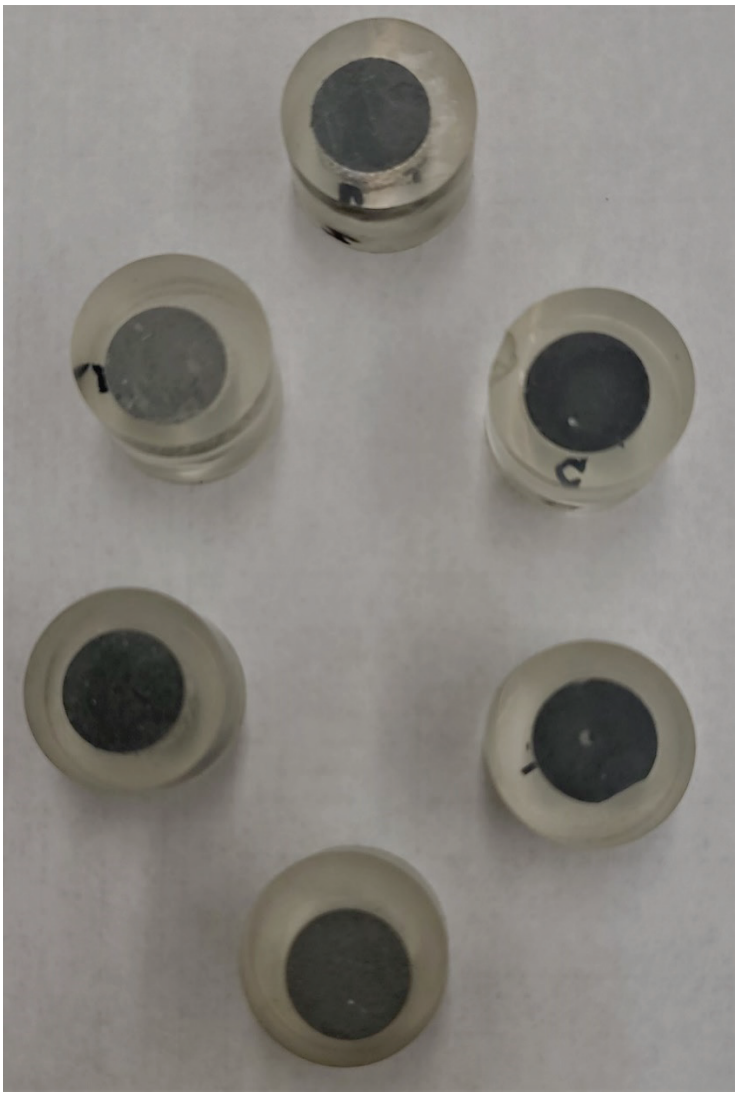

Figures 28 through 34 show SEM images of 0.3% and 0.9% CGG-based cement paste and reference (without graphene). All samples were obtained by high-shear-rate mixing in the presence of MasterGlenium 7920 dispersant or HRWRA.

Figure 28. CGG-based cement paste, 0.3% graphene, at 77× magnification.

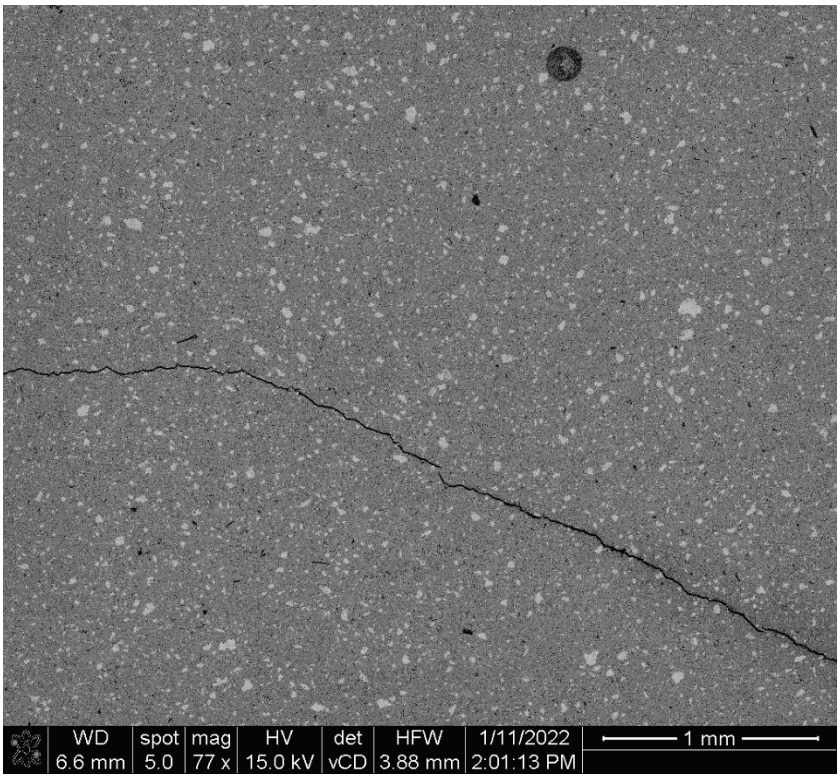

Figure 29. CGG-based cement paste, 0.3% graphene, at 2,000× magnification.

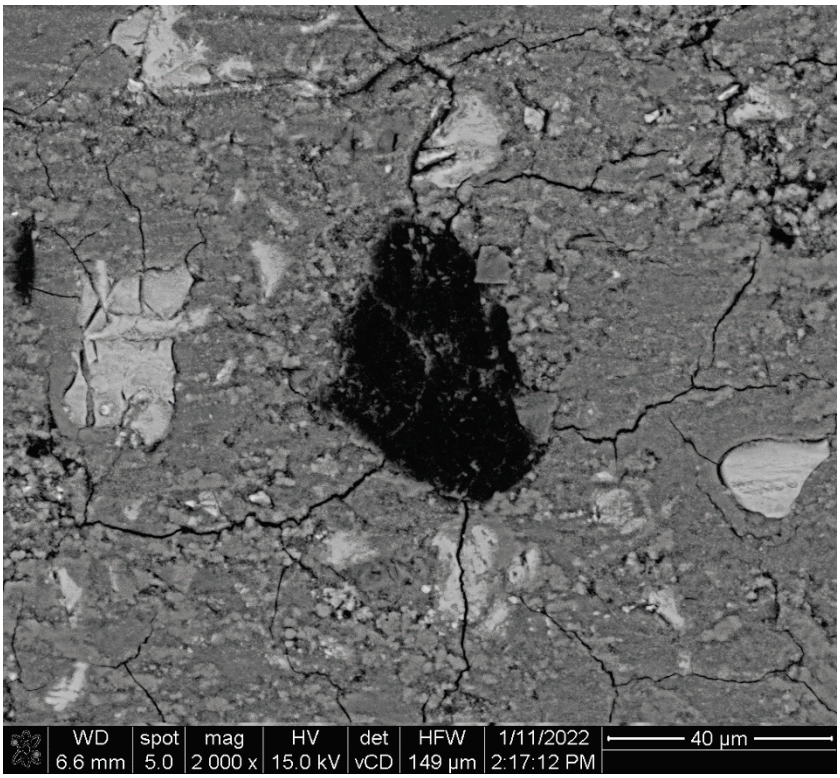

Figure 30. CGG-based cement paste, 0.9% graphene, at 77× magnification.

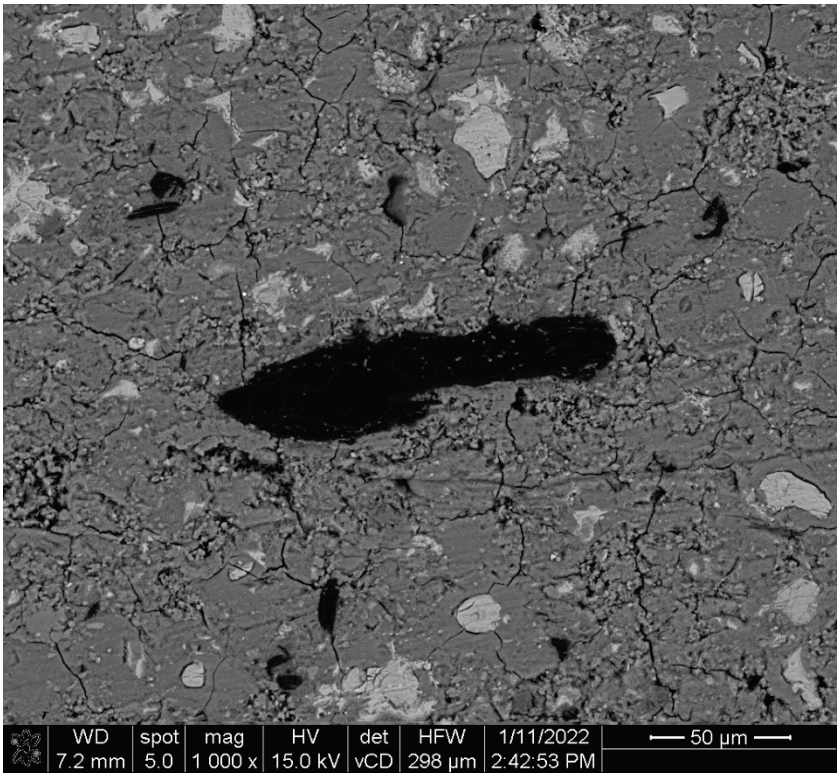

Figure 31. CGG-based cement paste, 0.9% graphene, at 2,000× magnification.

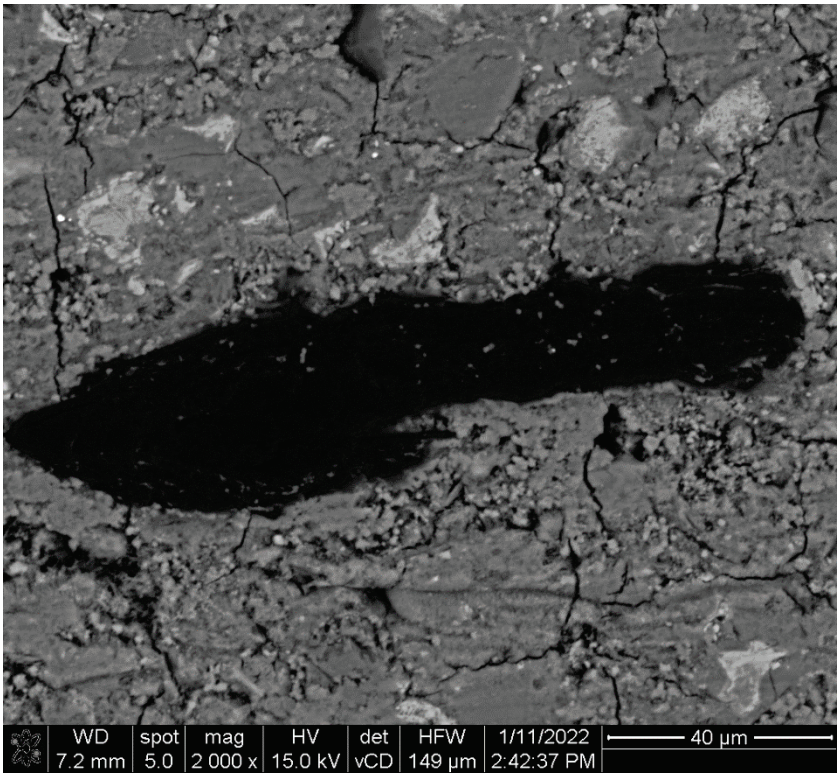

Figure 32. Reference cement paste without graphene at 77× magnification.

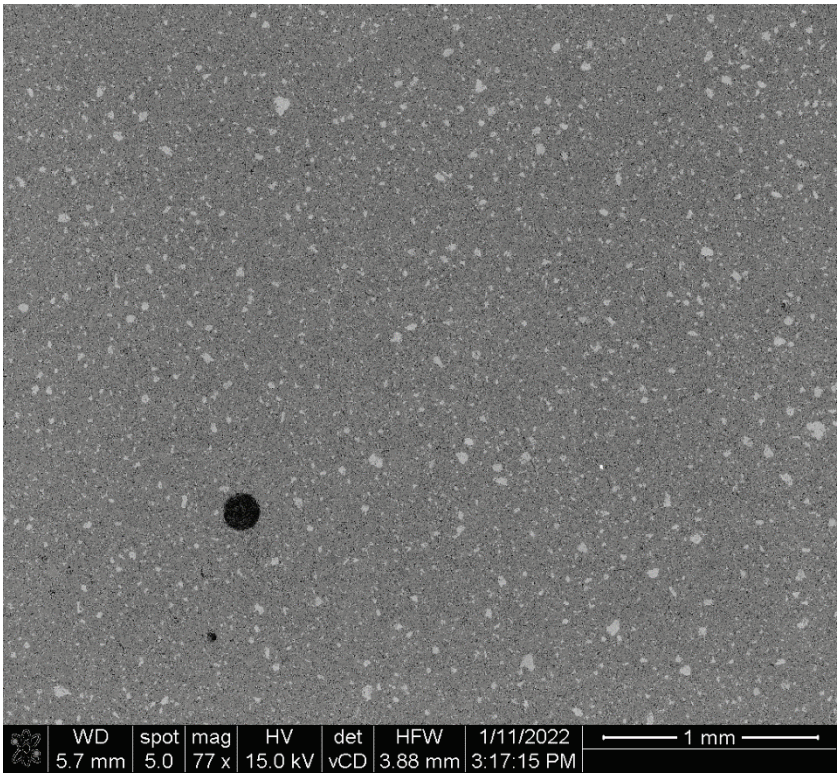

Figure 33. Reference cement paste without graphene at 1,000× magnification.

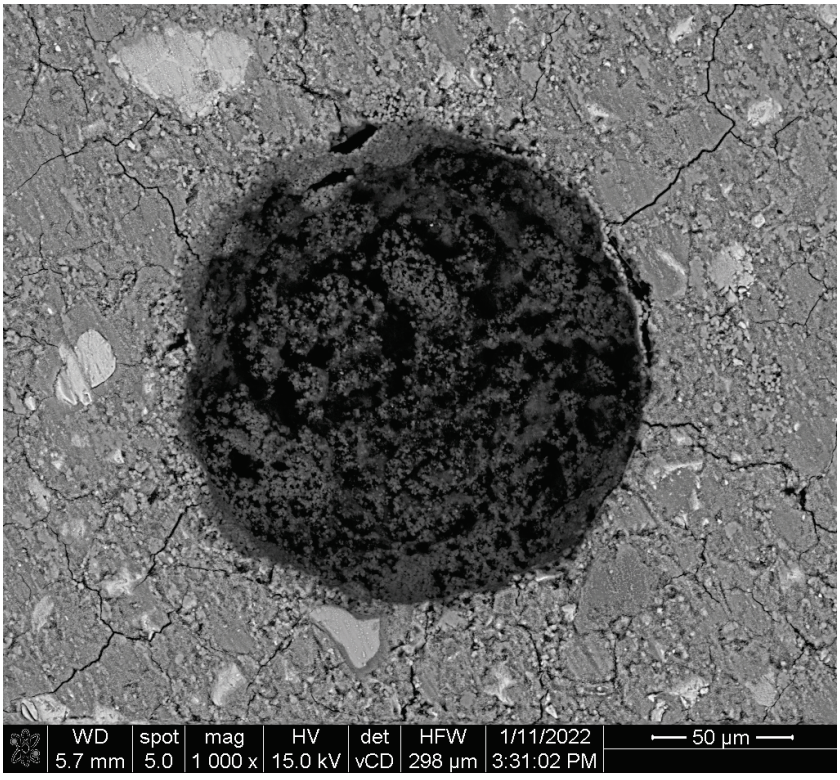

Figure 34. Reference cement paste without graphene at 2,000× magnification.

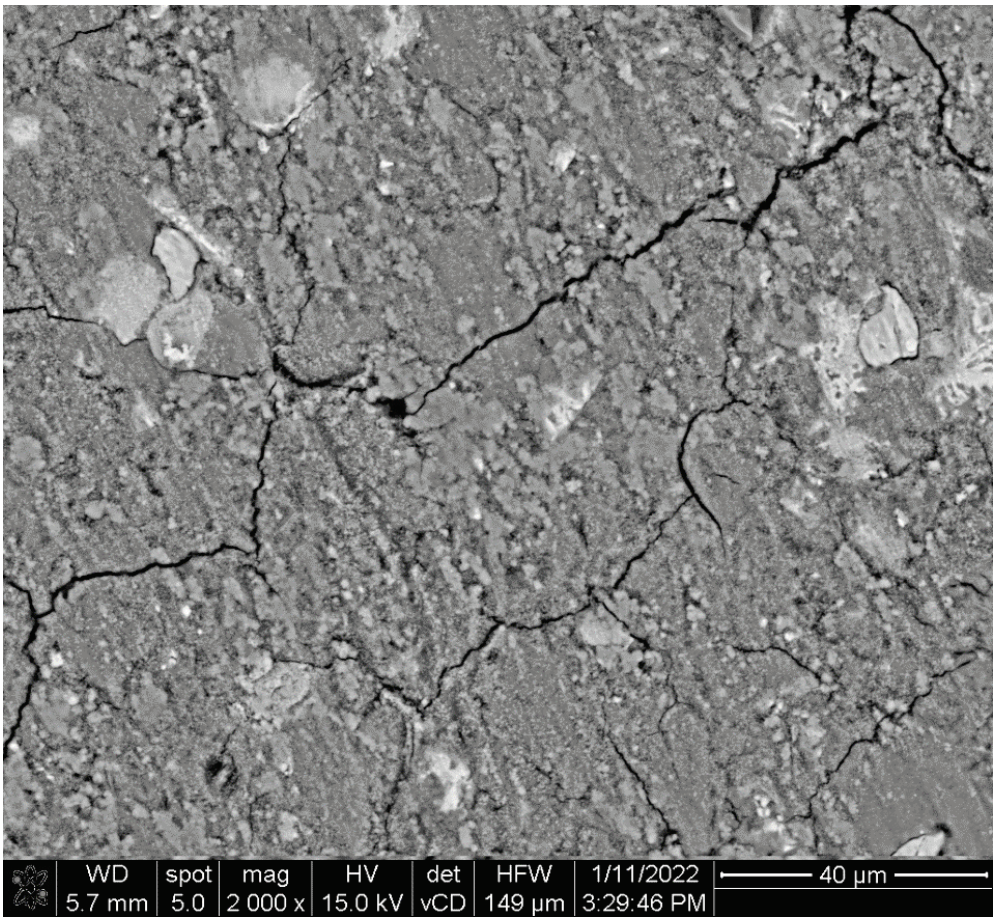

Figures 35 and 36 show SEM images of 0.3% graphene cement pastes obtained through high-shear-rate mixing without dispersant.

Figure 35. High shear rate mixed CGG-based cement paste, 0.3% graphene, no dispersant, at 77× magnification.

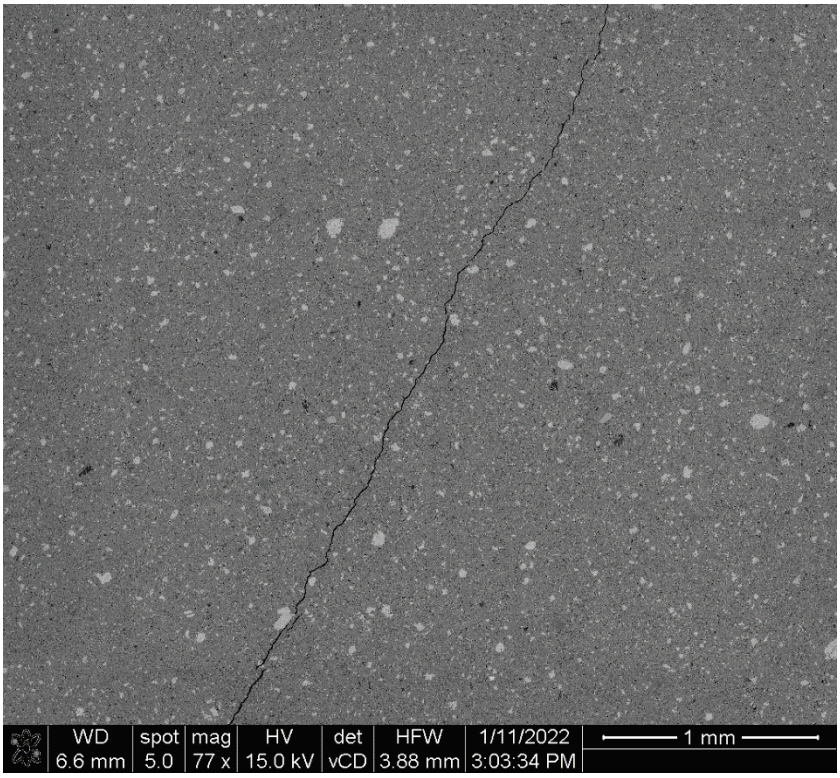

Figure 36. High shear rate mixed CGG-based cement paste, 0.3% graphene, no dispersant, at 2,000× magnification.

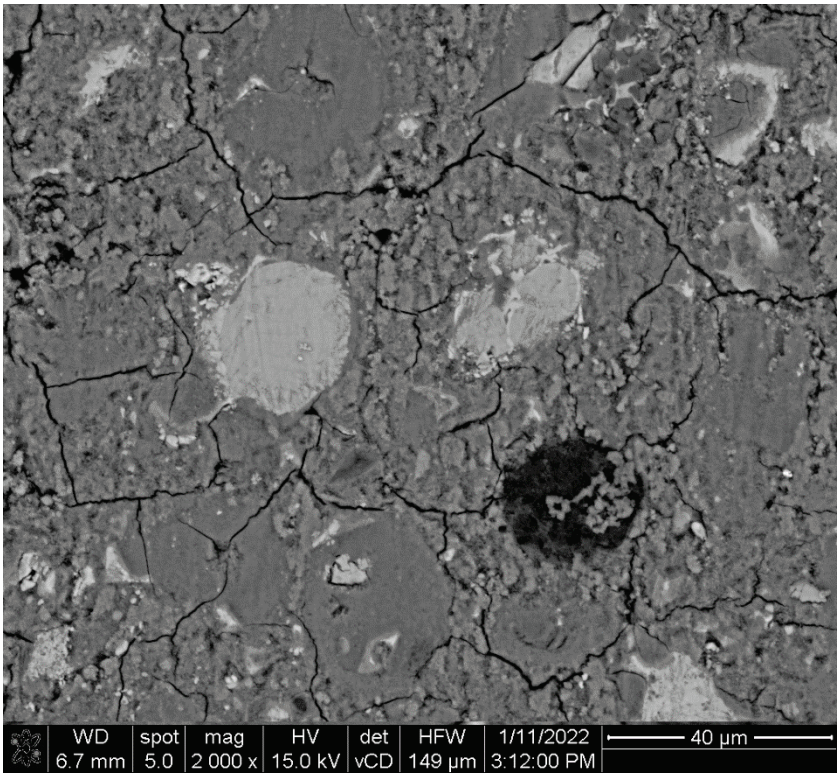

Following the benchtop SEM/EDS analyses of nonpolished graphene-cement and reference materials, similar experiments were repeated for polished samples using a higher resolution SEM/EDS instrument pair for elemental mapping. An elemental map was drawn for the circled area shown in Figure 37, and each element is presented with a different color as shown in Figure 38. Carbon EDS is shown in as an example to elemental analysis of graphene-cement mixtures in Figure 39, and Figure 40 shows the elemental composition analysis map.

Table 5 presents all the elements found in the graphene-cement microstructure along with their mass and atomic concentration percentages. Appendix A shows EDS map of each individual element in CCG-based 0.3% graphene cement paste.

Figure 37. SEM/EDS image of high shear rate mixed CGG-based cement paste, 0.3% graphene, with dispersant, at 498× magnification.

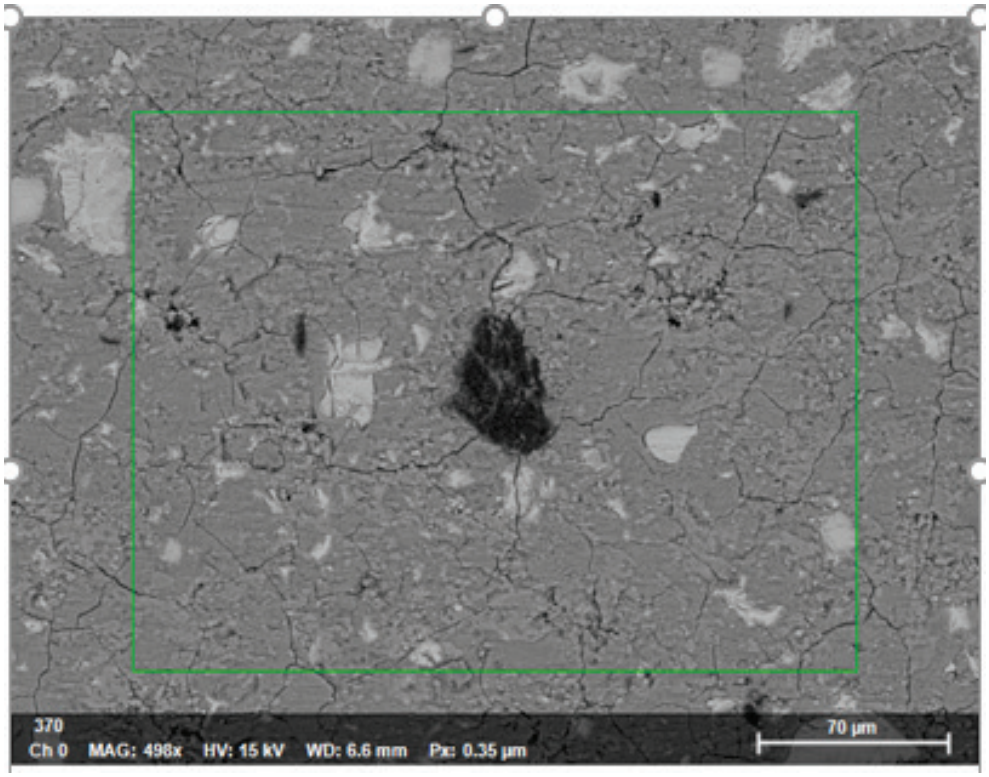

Figure 38. EDS chemical microstructure analysis of high shear rate mixed CGG-based cement paste, 0.3% graphene, with dispersant, at 498× magnification.

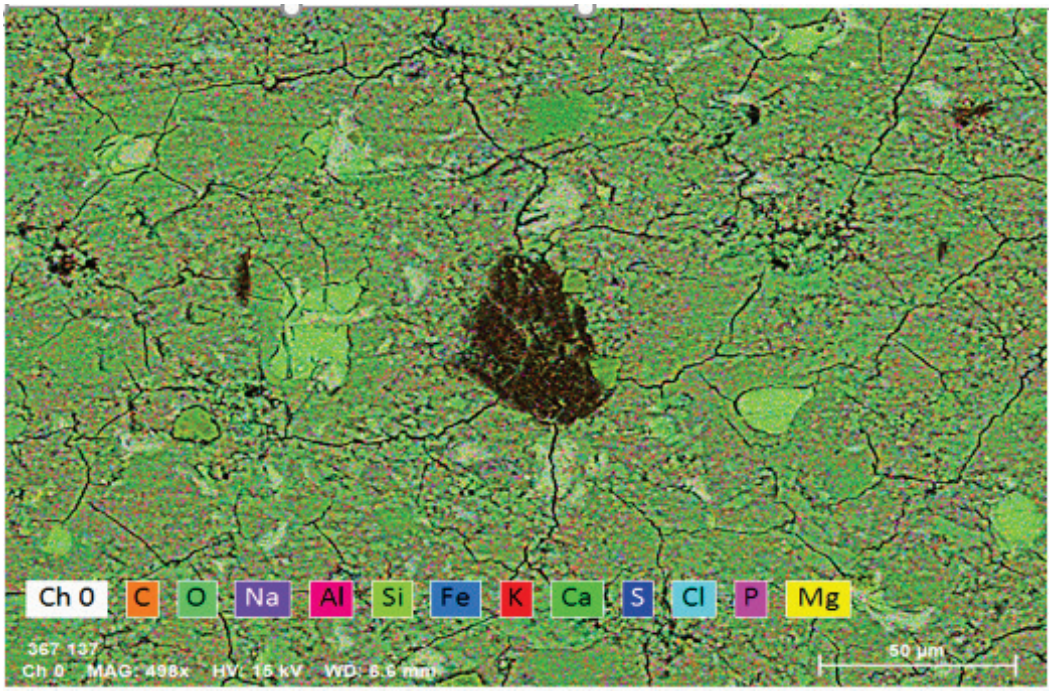

Figure 39. EDS chemical microstructure analysis for carbon in CGG-based cement paste with 0.3% graphene.

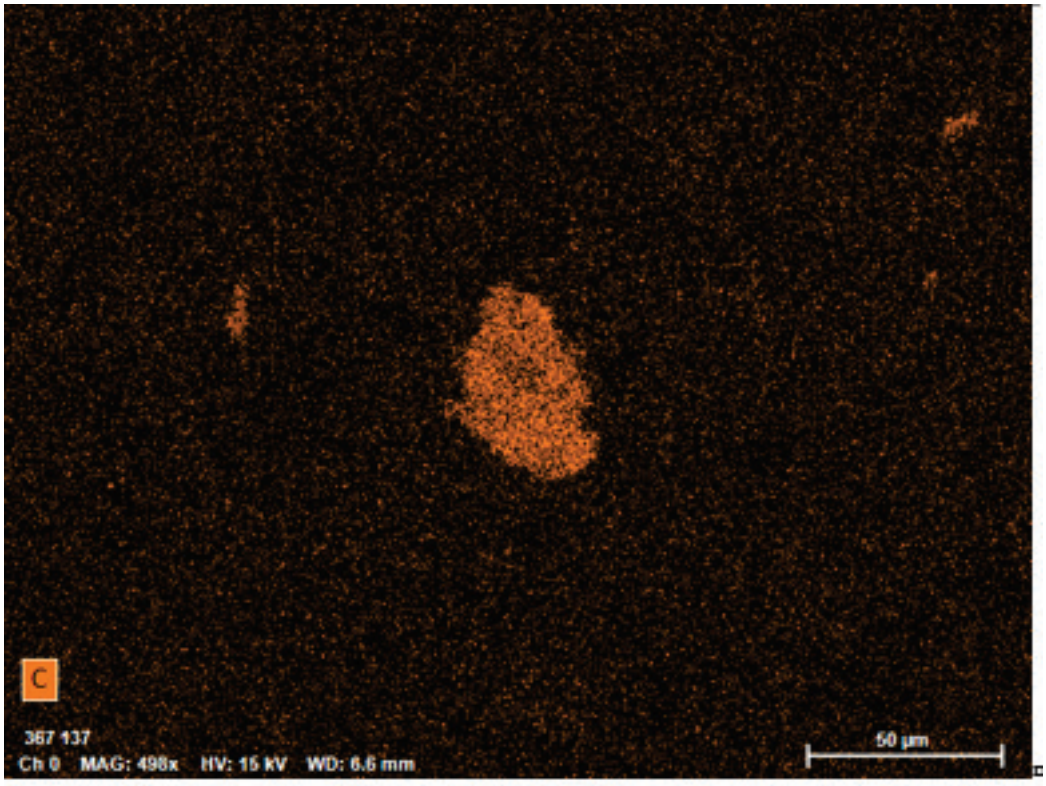

Figure 40. EDS elemental composition analysis map for CGG-based cement paste with 0.3% graphene.

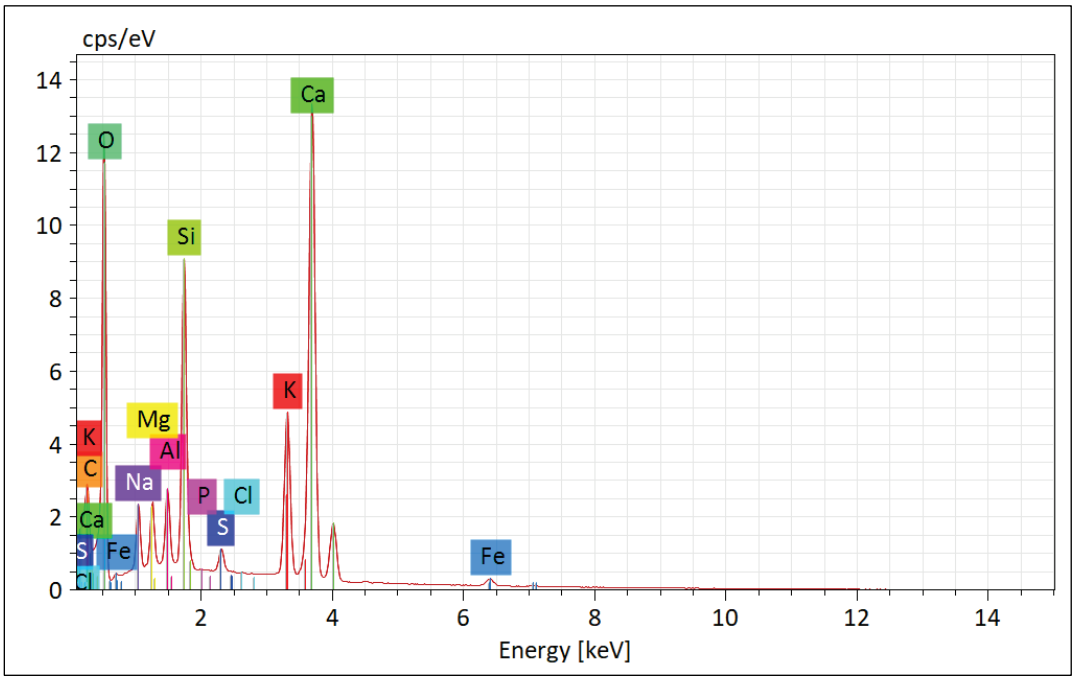

Table 5. EDS Elemental composition for CGG-based cement paste with 0.3% graphene.

Element	Atomic Number	Netto	Mass [%]	Mass Norm [%]	Atom [%]	Abs. Error [%] (1 sigma)	Rel. Error [%] (1 sigma)
Oxygen	8	241099	13.51	49.77	59.61	1.49	11.00
Calcium	20	448342	4.40	16.21	7.75	0.16	3.54
Silicon	14	219237	3.95	14.55	9.93	0.19	4.79
Carbon	6	42197	2.56	9.44	15.07	0.33	12.92
Sodium	11	32613	0.95	3.51	2.92	0.08	8.88
Aluminum	13	43119	0.82	3.03	2.15	0.06	7.72
Magnesium	12	32307	0.70	2.58	2.03	0.06	8.92
Sulfur	16	11921	0.25	0.91	0.55	0.03	13.79
Iron	26	0	0.00	0.00	0.00	0.00	0.92
		Sum	27.14	100.00	100.00		

Figure 41 shows powder XRD analysis of the cement-containing graphene showing peaks centered at 26.5˚ corresponding with the (002) peak of the graphene. This peak is not present in the reference (control) samples, as expected. Similarly, as the graphene percentage is increased from 0.3% to 0.9%, the intensity of the (002) peak increases substantially.

Figure 41. Powder XRD of reference paste and 0.3% and 0.9% graphene in CGG-based cement pastes.

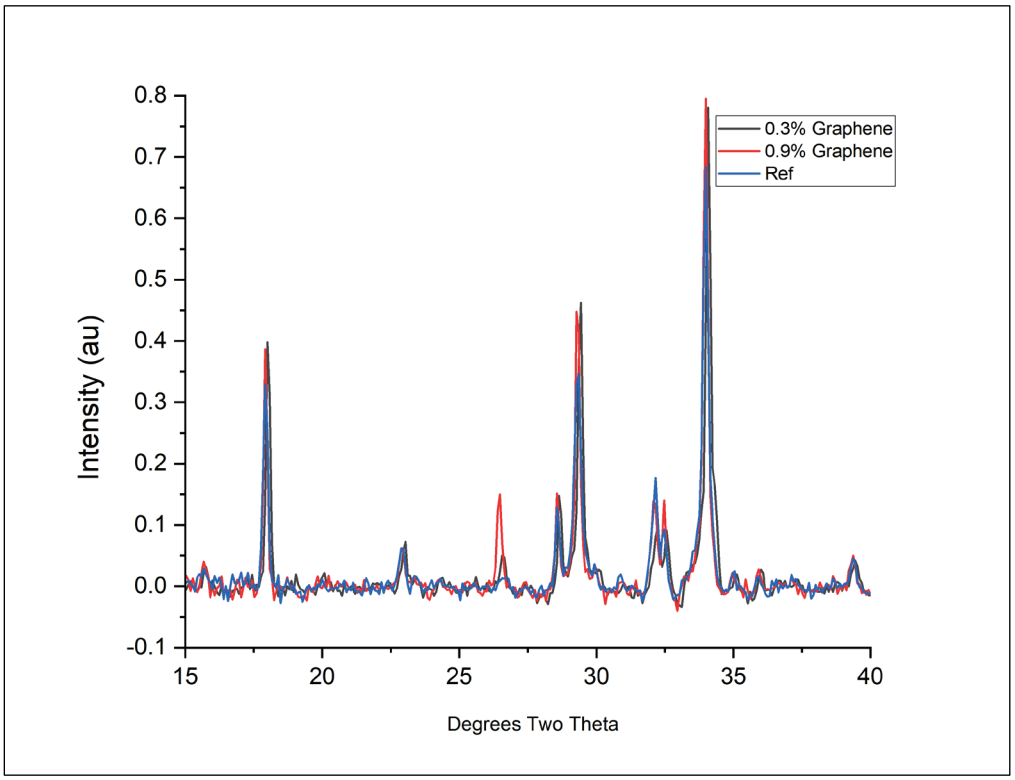

Figure 42 presents powder XRD analysis of the reference and 0.3% graphene in CGG-based cement paste, where addition of dispersant on the lattice structure of cement paste was investigated. Based on this study, no major change was observed in the graphene-cement lattice structure due to the addition of dispersant.

Figure 42. Powder XRD of reference paste and 0.3% CGG-based cement pastes with and without dispersant in the presence of high-shear-rate mixing.

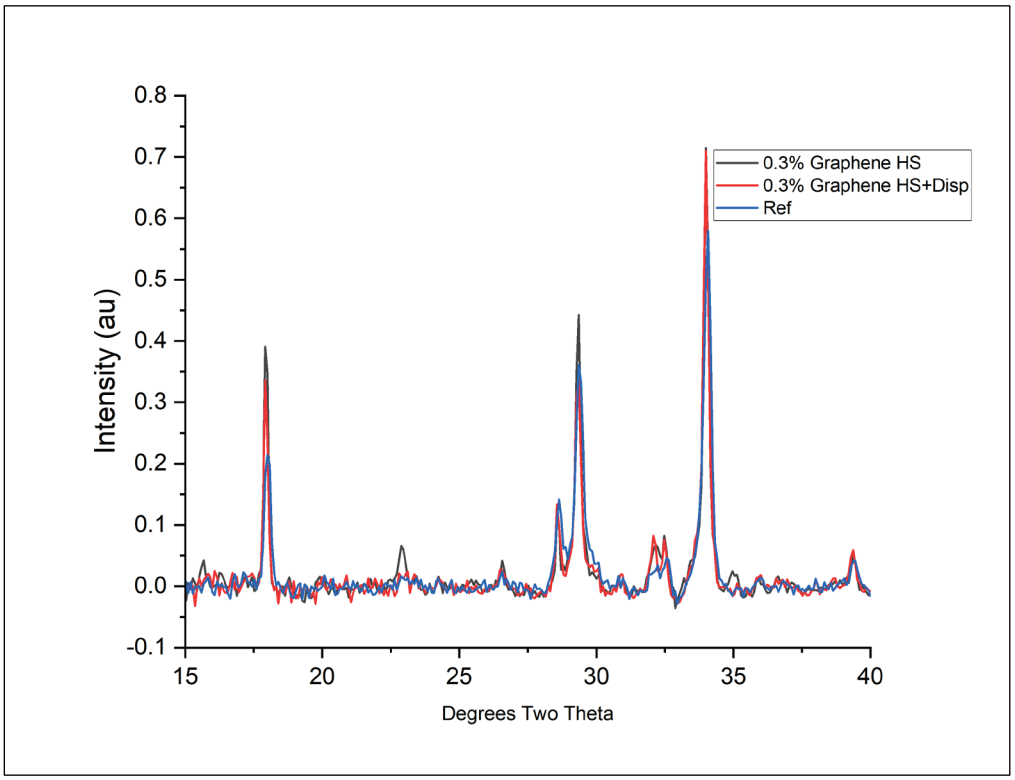

Figure 43 shows the Raman spectra of reference paste, 0.3%, and 0.9% graphene percentages of CGG-based cement pastes. D, G, and 2-D peaks were observed in the graphene containing samples. However, some peaks close to the location of the D, G and 2-D peaks are present in the control samples. These peaks present in the control samples are not easily identifiable in literature, but they can be differentiated from peaks resulting from graphene due to their decreased intensity, not sharing the same intensity ratio as the graphene has, as well as having slightly different Raman shifts. For example, the G peak in the graphene containing samples is centered at ~1575 cm^{-1}, whereas the unknown peak in the cement control samples is centered at ~1595 cm^{-1}. However, these unknown peaks innate to the cement matrix material do clearly cause some peak broadening of the D, G, and 2-D peaks, which increase the full width at half maximum (FWHM) of these peaks. Peaks occurring below ~1340 cm^{-1} originate from the cement matrix material, a mixture of crystalline oxides and carbonates. The most intense peak, centered at 1084 cm^{-1}, likely results from the carbonate stretching.

Figure 44 presents the XPS spectra of xGnP® grade C-750 and BF-103. Graphene and graphite samples show high carbon content and some surface oxygen content. The high-resolution scans of the C1s (tall peaks) and O1s (short peaks) regions can be used to give a better understanding of the interactions taking place at the exposed surface of the ground samples. Based on the XPS results, higher oxygen content was found in the xGnP©C-750 graphene compared to BW graphite.

Figure 43. Raman spectra of reference paste, and 0.3% and 0.9% graphene in CGG-based cement pastes.

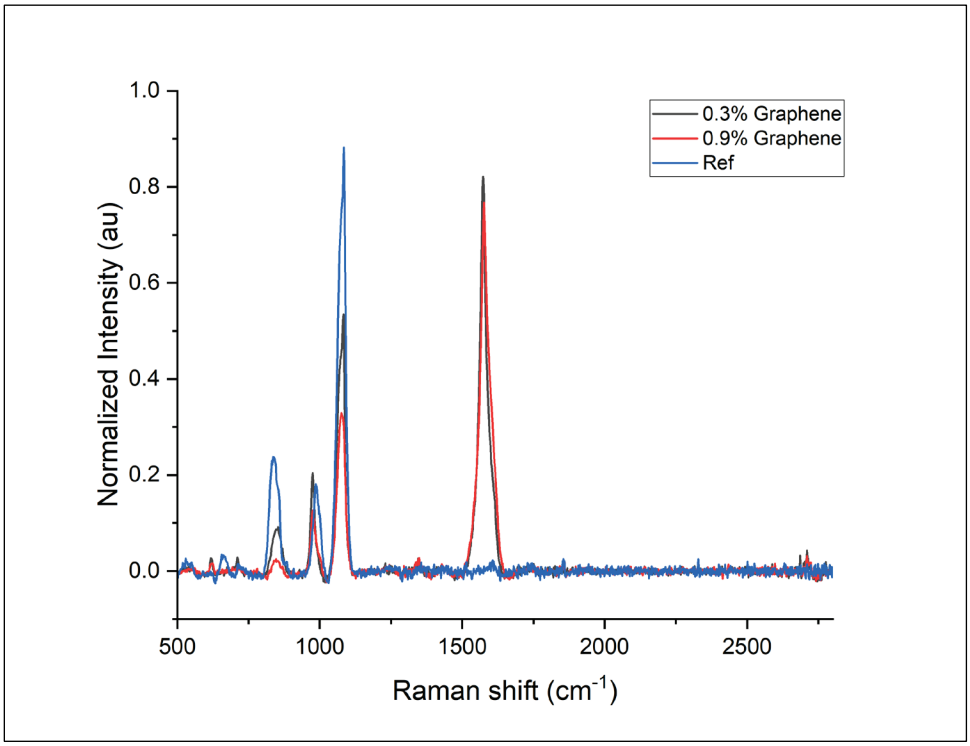

Figure 44. XPS spectra of xGnP® grade C-750 and BF-103.

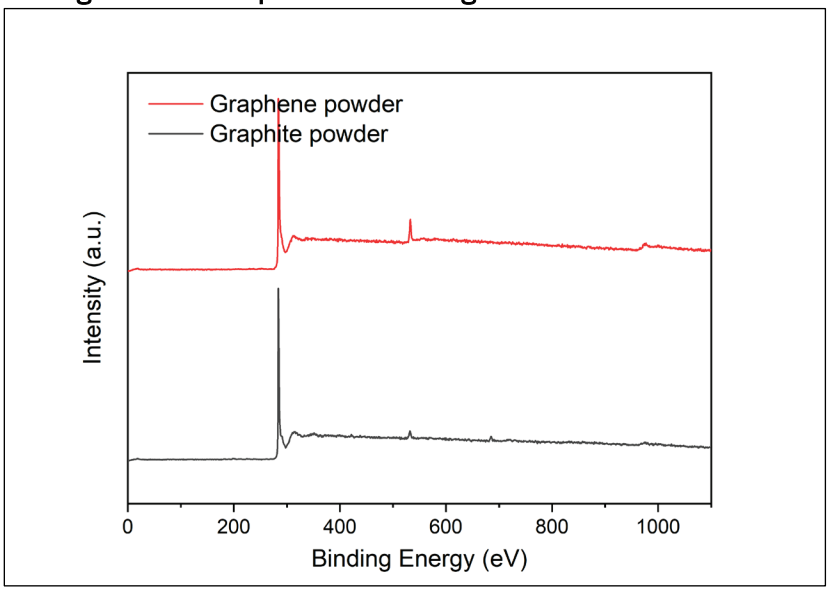

Figure 45 shows FTIR analysis of reference paste, and 0.3% and 0.9% graphene in CGG-based cement pastes. The peaks observed for carbonates at 870 cm^{-1}, Si-O stretching at 961 cm^{-1}, and two broad overlapping peaks at 1390 cm^{-1} and 1490 cm^{-1} can also be attributed to the carbonates present in the cement. As graphene has no asymmetry, it cannot be detected using FTIR. The use of surfactant also is not detected in any meaningful way, likely because it is not present in high enough concentrations on the surface of the sample to be detected by the instrument.

Figure 45. FTIR spectra of reference paste, and 0.3% and 0.9% graphene in CGG-based cement pastes.

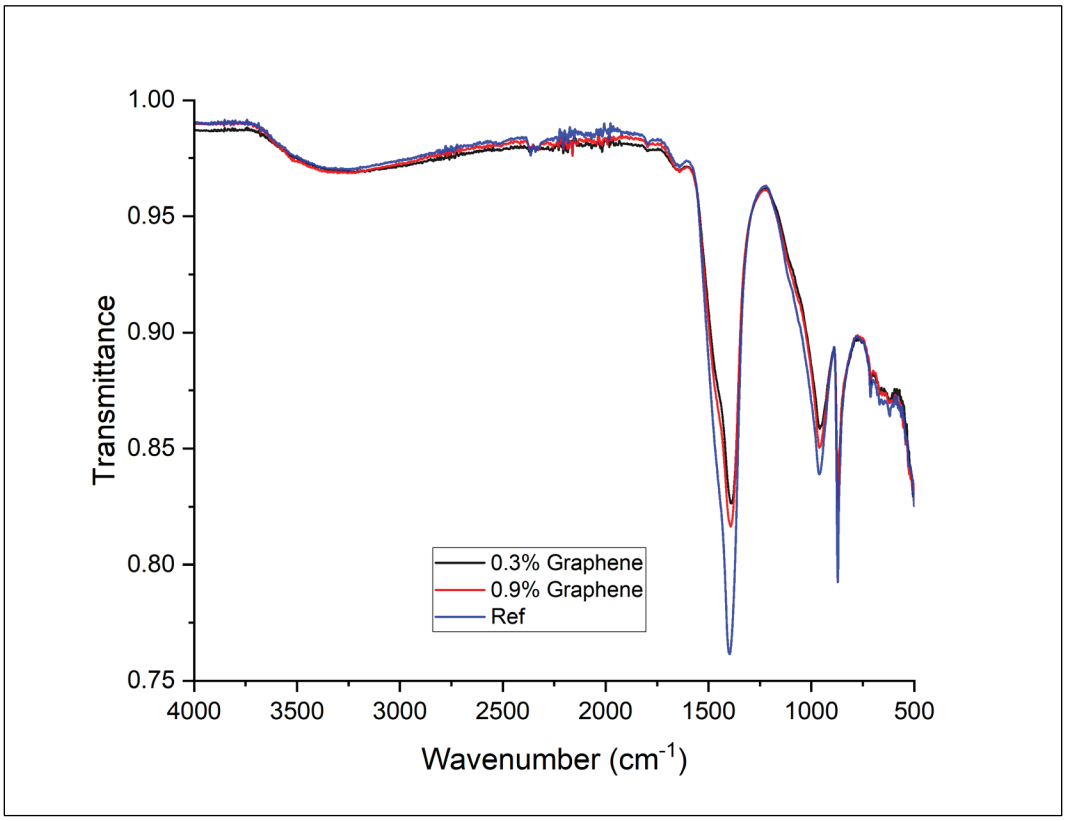

3 Discussion on Test Results of Laboratory-Generated Graphene (LGG) and Commercial-Grade Graphene (CGG) in Cementitious Materials

LGG- and CGG-based cement pastes provided higher compressive strength than the reference paste at 7- and 14-day curing duration as presented in Figure 11 to 16. However, after 14 days of curing, the increase in compressive strength becomes minimal for LGG-based cement pastes and seems to stabilize for CGG-based cement pastes. In addition, 0.3% graphene loaded CGG-based cement paste shows an increase in compressive strength from seven to 28 days. This noted increase in compressive strength for 7-, 14-, 28-day curing duration, provides an opportunity for utilization in numerous civilian and military applications.

The white calcite formation observed on the samples with lower percentages of LGG (Figure 17), were analyzed using SEM/EDS. Based on the SEM/EDS and visual inspection, the top faces of all these cubes—in direct contact with air—presented a high percentage of calcite formation. This observation, when compared to the samples with higher percentages of LGG- and CGG where minimal to no calcite formation was observed, points out the importance of dispersant dosage used in preparing graphene cement paste. In the preparation of the LGG-based-cement pastes a higher amount of dispersant dosage was used compared to the CGG-based-cement-pastes.

XPS allows quantitative analysis of elemental content and binding at the surface of the material. Graphene and graphite samples show high carbon content and some surface oxygen content. The high-resolution scans of the C1s and O1s regions can be used to give a better understanding of the interactions taking place at the exposed surface of the ground samples. Based on the XPS results, more oxygen content was found in the xGnP©C-750 graphene compared to BA graphite.

Researchers found that it was important to use the correct shear rate in the presence of dispersant to avoid agglomeration and achieve effective graphene dispersion in the cement matrix. It should also be noted that because of the energy dissipation in high-shear-rate mixing,

a temperature increase in the stabilized aqueous graphene dispersion solutions was observed.

Based on the SEM microstructural analyses, higher compressive strength graphene-cement mixtures were found to have better microstructure patterns with much finer or reduced crack formation as observed qualitatively. SEM images show that in the graphene-cement composite matrices, cracks are stopped in the presence of graphene sheet, whereas in ordinary matrices cracks seem to continue in the form of a straight line.

4 Conclusions and Recommendations

This study establishes a baseline for understanding the influence of graphene in cementitious materials and presents a solid basis for the future development of graphene-cement mortar and graphene-concrete composites leading to sustainable structures with lower carbon footprint when compared to legacy concrete.

Graphene-cement paste processing parameters including the dispersant and its dosage, graphene percentage, and mixing method were studied to optimize the LGG- and CGG-based cement pastes with higher compressive strength compared to cement pastes without graphene. Graphene dispersion in the cement matrix was optimized by analyzing the effect of high-shear-rate mixing and the presence of dispersant in the stabilized aqueous solution for homogeneous graphene-cement paste matrices. The calcite formation was investigated for lower graphene percentage LGG-cement pastes during curing and compared to higher percentages of LGG and CGG-based pastes. Mechanical, chemical, and microstructural properties of LGG- and CGG-based cement pastes were analyzed using XPS, XRD, FTIR, Raman spectroscopy, and SEM/EDS and a correlation between microstructure and compressive strength was determined.

Further exploration of graphene in cementitious matrices will facilitate adoption of GRM for military construction, warfighter support, fighting climate change, and use in our nation's vast civil works infrastructure.

4.1 Conclusions

This research demonstrates that it is possible to obtain graphene-cement pastes with higher compressive strength compared to their reference pastes. These findings point out the importance of achieving optimum graphene dispersion in the cementitious media that is determined by the type of dispersant, the rate of high-shear-rate mixing, along with graphene type, size, and dosage rate. Effective graphene dispersion was achieved when the graphene particle size was less than 2 μm with a surface area of 750 m^2/g for xGnP® C-750, and 4.6 to 27.2 μm particle size range with a surface area of 1 m^2/g for BF-103, where shear rate was kept at 5,000 rpm. The findings of this report are expected to be the starting point for graphene-cement mortar and graphene-cement concrete composite

studies where additives such as fine and coarse aggregates are added, respectively, to make the graphene-cement composites.

Graphene-cement pastes were prepared from LGG and CGG raw materials with ASTM Type I/II portland cement. Chemical structure, microstructure, and mechanical strength of LGG and CGGs were studied to map graphene-cement paste structure/processing/property relationships. Using these relationships, parameters were established to achieve the highest compressive strength. Graphene dosage, graphene particle size, speed of mixing, and dispersant agent were found to have important roles in determining the compressive strength of graphene-cement mixtures. This effect is a manifestation of graphene dispersion, which controls the adhesion forces between CSH gels and the graphene particle surfaces.

XPS, XRD, Raman, SEM/EDS analyses were used to determine the composites' chemical structure and microstructure. These properties along with the mechanical strength were used to map graphene-cement paste structure/processing/property relationships. At optimum graphene amounts, LGG- and CGG-based graphene cement mixtures showed an increase in compressive strength over 7-, 14-, and 28-day curing periods. Preliminary dispersion studies were performed to determine that MasterGlenium 7920 was the most effective surfactant for graphene dispersion. EDS elemental mapping confirmed that graphene was correctly incorporated into the graphene-cement paste formation. Furthermore, EDS results confirmed that using a higher dosage of dispersant results in more calcite formation at lower LGG percentages.

Optimum graphene dosage was determined by studying various graphene percentages in cement mixtures and completing their chemical, microstructural, and mechanical analyses. Knowledge of optimum dosage is imperative to prevent agglomerations. In cement mixture preparations when the dosage is above a certain threshold, agglomeration occurs and causes many layers of graphene to come together and form multi layers of graphene. As a result of these multi layers, and weak van der Waals interactions, friction force between graphene and cementitious material is reduced and results in debonding and displacement of layers that reduces the strength of graphene-cement mixtures.

4.2 Recommendations

In the future, fabrication of graphene-mortar and graphene-concrete composites will continue to impact of fine and coarse aggregates on the physio-mechanical behavior of the graphene-concrete materials. One can expect to see significant improvements in graphene-concrete over conventional concrete in tensile and flexural applications where the tensile strength and Young's modulus of graphene will be utilized better.

In addition, the effect of calcite and particle size on the mechanical performance of graphene-cement composites; decrease in compressive strength after 14-day curing; additional mechanical tests such as tensile and flexural strength; dispersant effect on the graphene-cement composites through rheology; and temperature effect of stabilized aqueous graphene dispersion in the cement mixture preparation will be studied to determine graphene-cement composite performance. Furthermore, morphologies of graphene-cementitious materials and their long-term durabilities will be investigated along with computational tools for materials design of graphene-cement composites.

Exploring the opportunities in the use of graphene will allow for better-performing structures in military engineering under blast and penetration situations. Further investigation of graphene in cementitious matrices will facilitate adoption of GRM for military construction, warfighter support, fighting climate change, and use in our nation's vast civil works infrastructure.

References

ASTM. 2017. *Standard Practice for Fabricating and Testing Specimens of Ultra-High Performance Concrete*. C1856/C1856M-17. West Conshohocken, PA: ASTM International.

ASTM. 2019. *Standard Specification for Portland Cement*. C150/C150M-19. West Conshohocken, PA: ASTM International.

ASTM. 2021a. *Standard Test Method for Compressive Strength of Cylindrical Concrete Specimens*. C39/C39M-21. West Conshohocken, PA: ASTM International.

ASTM. 2021b. *Standard Test Method for Compressive Strength of Hydraulic Cement Mortars (Using 2-in. or [50 mm] Cube Specimens)*. C109/C109M-21. West Conshohocken, PA: ASTM International.

Dimov, D., I. Amit, O. Gorrie, M. D. Barnes, N. J. Townsend, Ana I. S. Neves, Freddie Withers, Saverio Russo, and Monica Felicia Craciun. 2018. "Ultrahigh Performance Nanoengineered Graphene–Concrete Composites for Multifunctional Applications." *Advanced Functional Materials* 28:1705183. **https://doi.org/10.1002/adfm.201705183.**

Drexler, K. E. 2004. "Nanotechnology: From Feynman to Funding." *Bulletin of Science, Technology, and Society* 24(1):21–27.

Du, H., and S. D. Pang. 2018. "Dispersion and Stability of Graphene Nanoplatalet in Water and Its Influence on Cement Composites." *Construction and Building Materials* 167:403–413.

Gronchi, P., S. Bianchi, L. Brambilla, and M. Goisis. 2018. "Graphite Nanoplatelets and Graphene Oxide Influence on C-S-H Formation." *ACI Symposium Publication* 329. **https://doi.org/10.14359/51711218**.

Hernandez, Y., V. Nicolosi, M. Lotya, F. M. Blighe, Z. Sun, and S. De. 2008. "High-Yield Production of Graphene by Liquidphase Exfoliation of Graphite." *Nature Nanotechnology* 3:563–568.

Ho, V. D., C.-T. Ng, T. Ozbakkaloglu, A. Goodwin, C. McGuckin, R. U. Karunagaran, and D. Losic. 2020. "Influence of Pristine Graphene Particle Sizes on Physicochemical, Microstructural, and Mechanical Properties of Portland Cement Mortars." *Construction and Building Materials* 264:120188.

Lea, F. M. 1970. *The Chemistry of Cement and Concrete*. New York, NY: Chemical Pub. Co.

Novoselov, K. S., A. K. Geim, S. V. Morozoy, D. Jiang, Y. Zhang, S. V. Durunos, I. V. Grigorieva, and A. A. Firsov. 2004. "Electric Field Effect in Atomically Thin Carbon Films." *Science* 306(5696):666–669. **https://doi.org/DOI: 10.1126/science.1102896.**

Xu, Y., H. Cao, Y. Xue, B. Li, and W. Cai. 2018. "Liquid-Phase Exfoliation of Graphene: An Overview on Exfoliation Media, Techniques, and Challanges." *Nanomaterials* 8(11):942.

Appendix A: Graphene-Related Materials (GRM) Specifications

Figure A-1. xGnP® grade C-750.

XGSciences®

xGnP® Graphene Nanoplatelets - Grade C

xGnP® Graphene Nanoplatelets are unique nanoparticles consisting of short stacks of graphene sheets having a platelet shape. Grade C particles are available in different grades that are designated by their approximate surface area.

Grade C particles typically consist of aggregates of sub-micron platelets that have a particle diameter of less than 2 microns and a typical particle thickness of a few nanometers, depending on the surface area. Grade C particles can be ordered with average surface areas of *300, 500, and 750 m^2/g*.

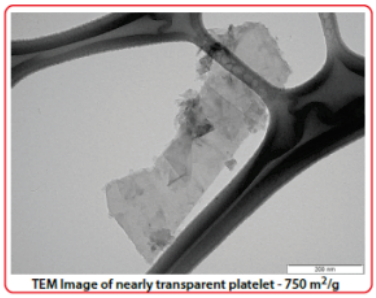

TEM Image of nearly transparent platelet - 750 m^2/g

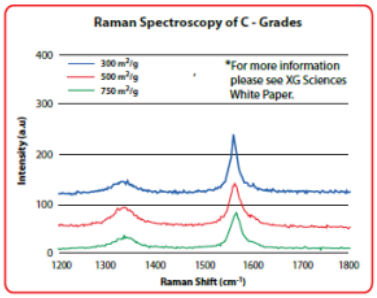

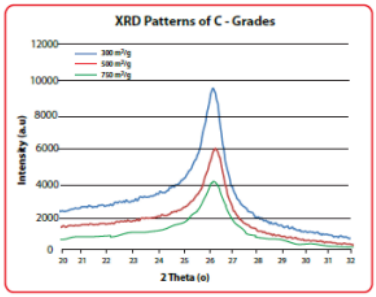

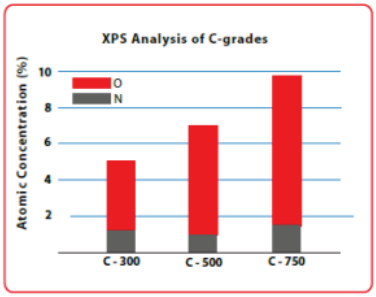

Characteristics of Bulk Powder

Property	*Typical Value*
Appearance	Black granules/powder
Bulk Density	0.2 to 0.4 g/cc
Relative Gravity	2.0-2.25 g/cc

**Note: nanoplatelets have naturally occurring functional groups like ethers, carboxyls, or hydroxyls that can react with atmospheric humidity to form acids or other compounds. These functional groups are present on the edges of the particles and their wt% varies with particle size.*

XG Sciences Inc.
3101 Grand Oak Drive
Lansing, MI 48911

+1 517 703 1110
info@xgsciences.com
www.xgsciences.com

Figure A-2. Barite World Graphite® BF-103.

BARITEWORLD
INDUSTRIAL MINERALS & CHEMICALS
Any application - Any industry - Any quantity

BariteWorld.com / Division Of Rockleigh Industries Inc.
8 Rockleigh rd, Rockleigh, New Jersey 07647 USA
Tel: +1 917-825-3806 / bariteworld@optonline.net
www.BariteWorld.com

Product Data Sheet

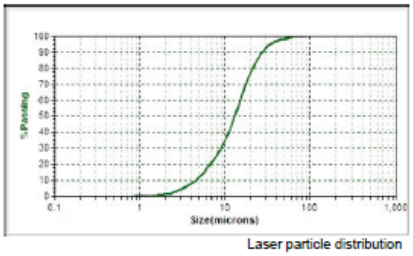

Laser particle distribution

Grade:
BF-103
Type: High Purity Natural Crystalline Flake Graphite

Specifications:

Size..... 99.0% min. -325 mesh
Carbon..... 99.0% Min.
Moisture..... 0.50% Max.

Typical Analysis:

Carbon..... 99.5%
Ash..... 0.5%
Moisture..... 0.10%
Bulk Density... 3.00g/in^3
Size..... 99.6% -325 mesh (passing 44µm)
test method - jet sieve. U.S. standard
D10 4.6 µm
D50 13.6 µm
D90 27.2µm
test method: Microtrac

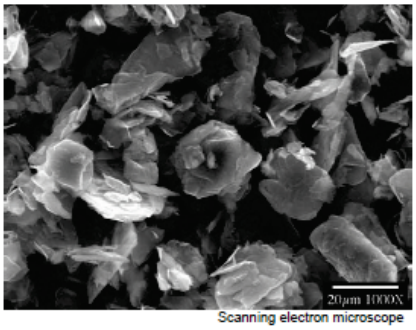

Scanning electron microscope

Rev. 10-1-08

Appendix B: SEM/EDS Analyses

Figure B-1. Color codes of elements in the map.

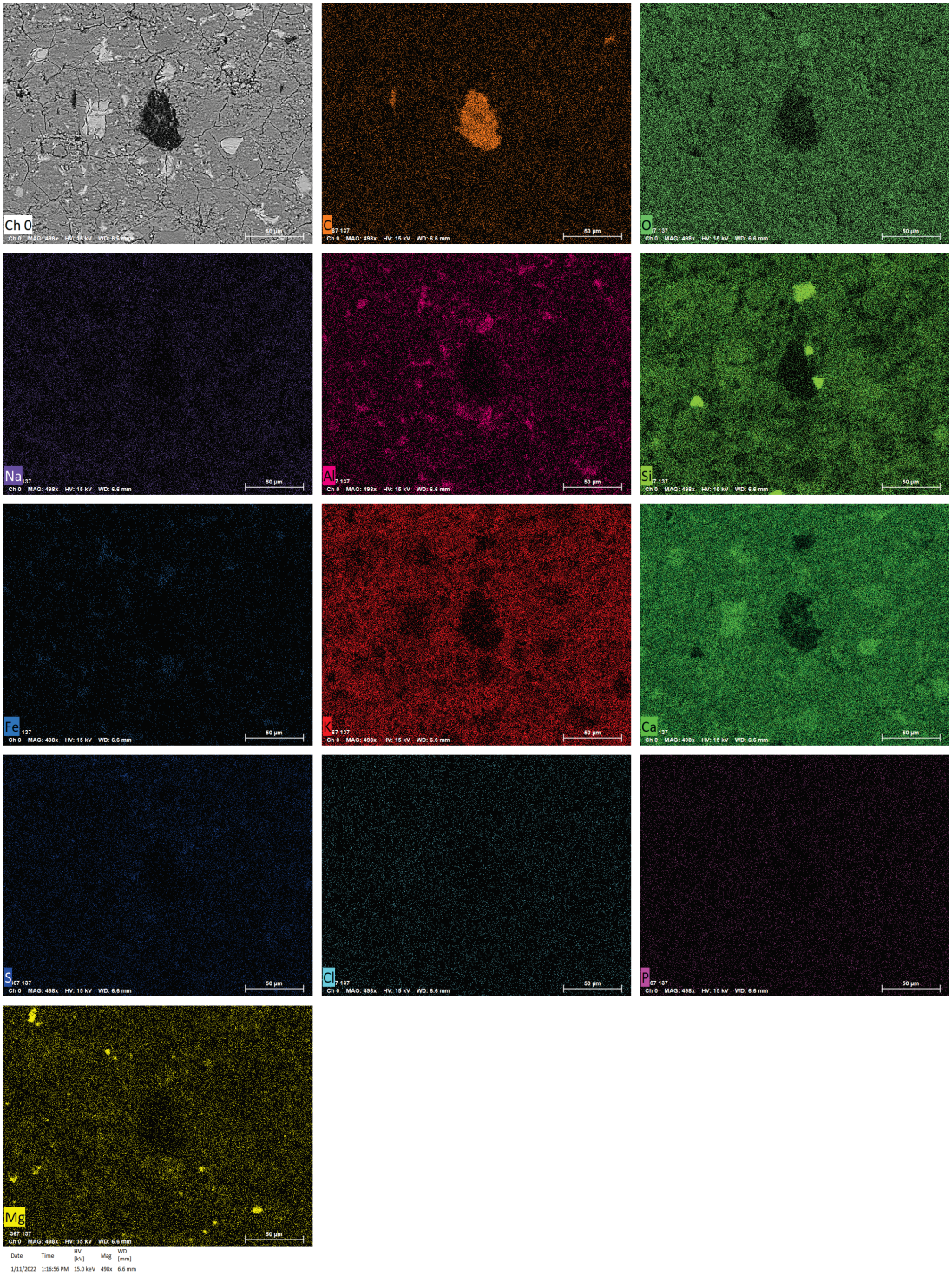

Figure B-2. EDS map of oxygen.

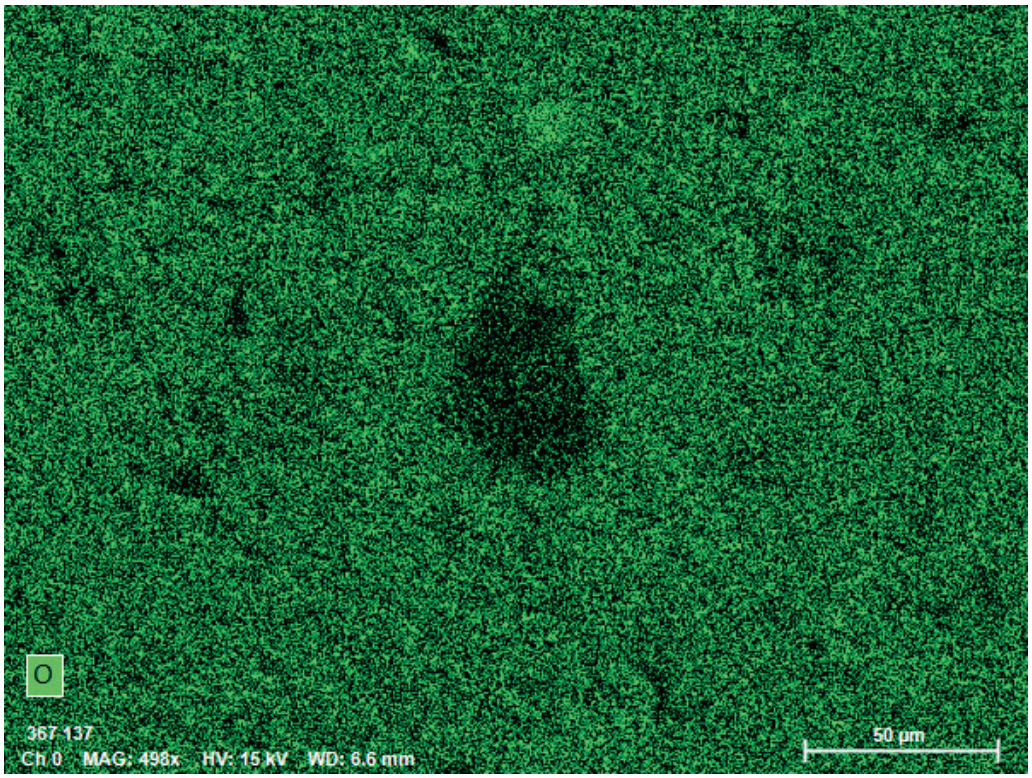

Figure B-3. EDS map of aluminum.

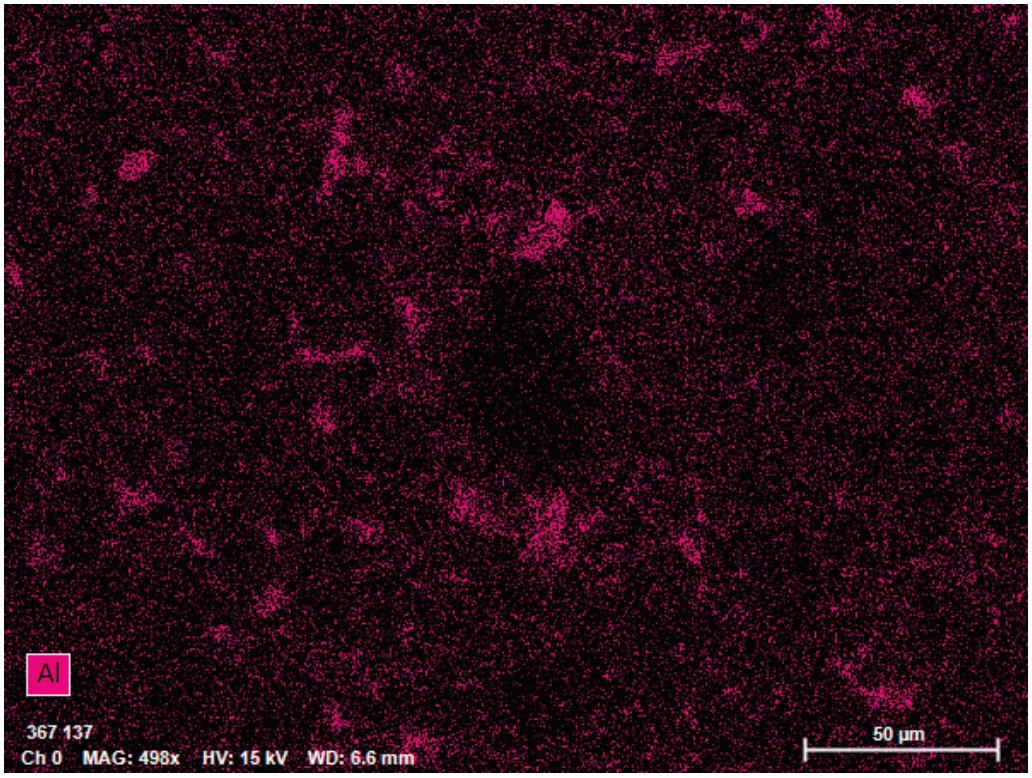

Figure B-4. EDS map of silicon.

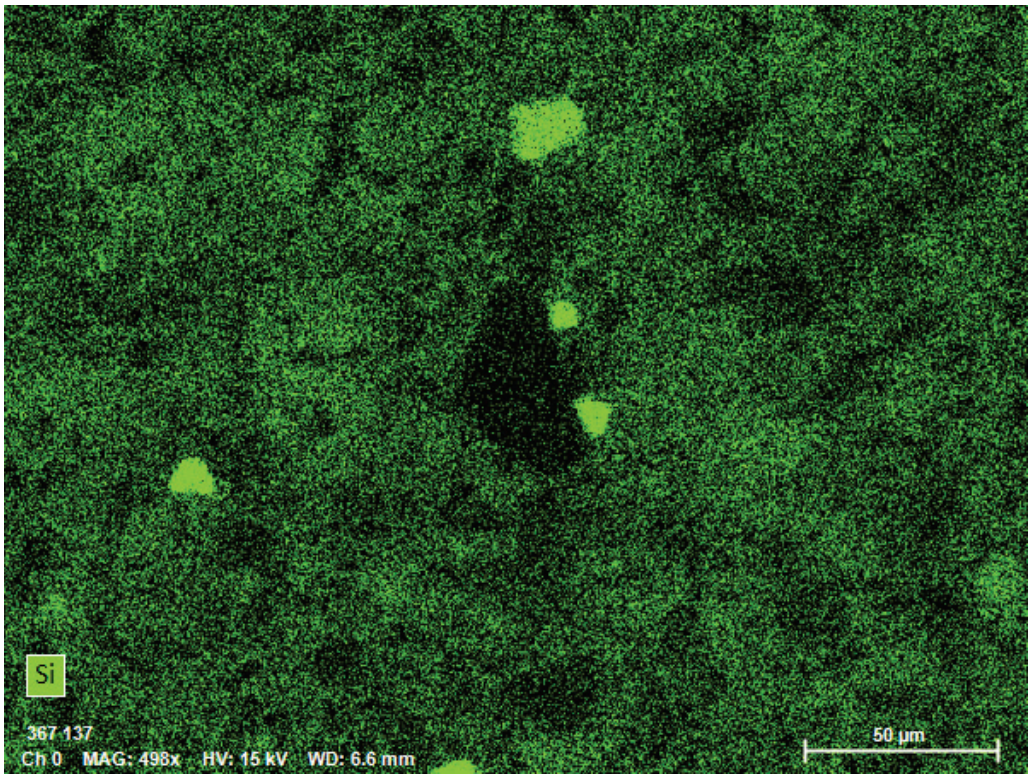

Figure B-5. EDS map of iron.

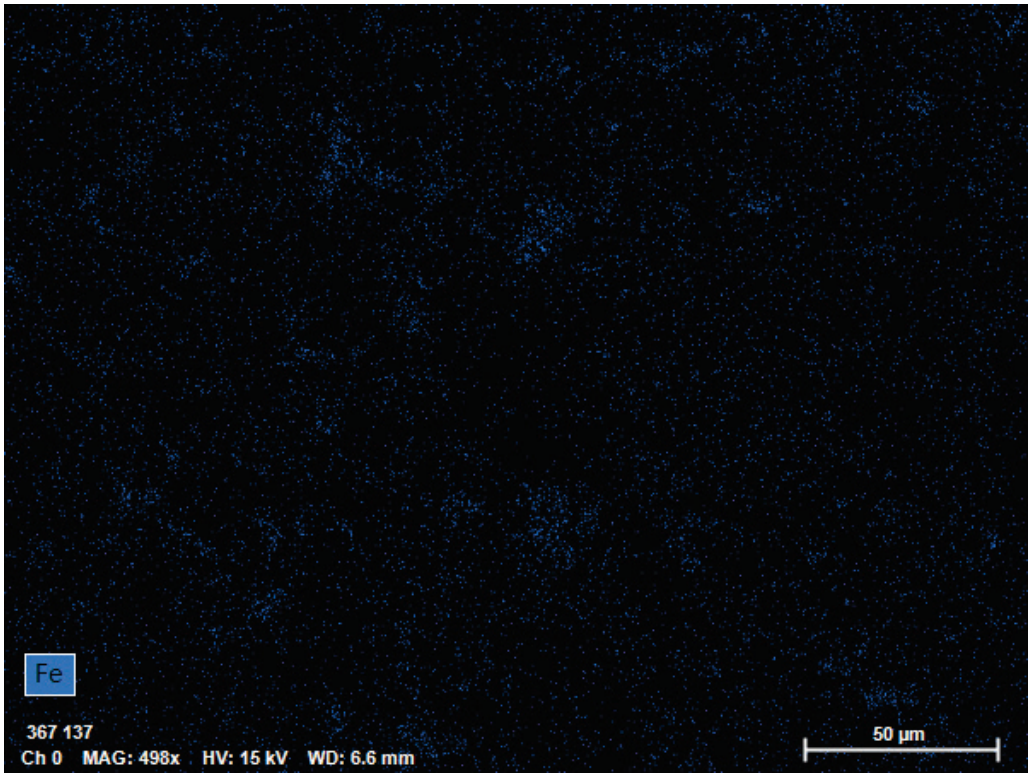

Figure B-6. EDS map of calcium.

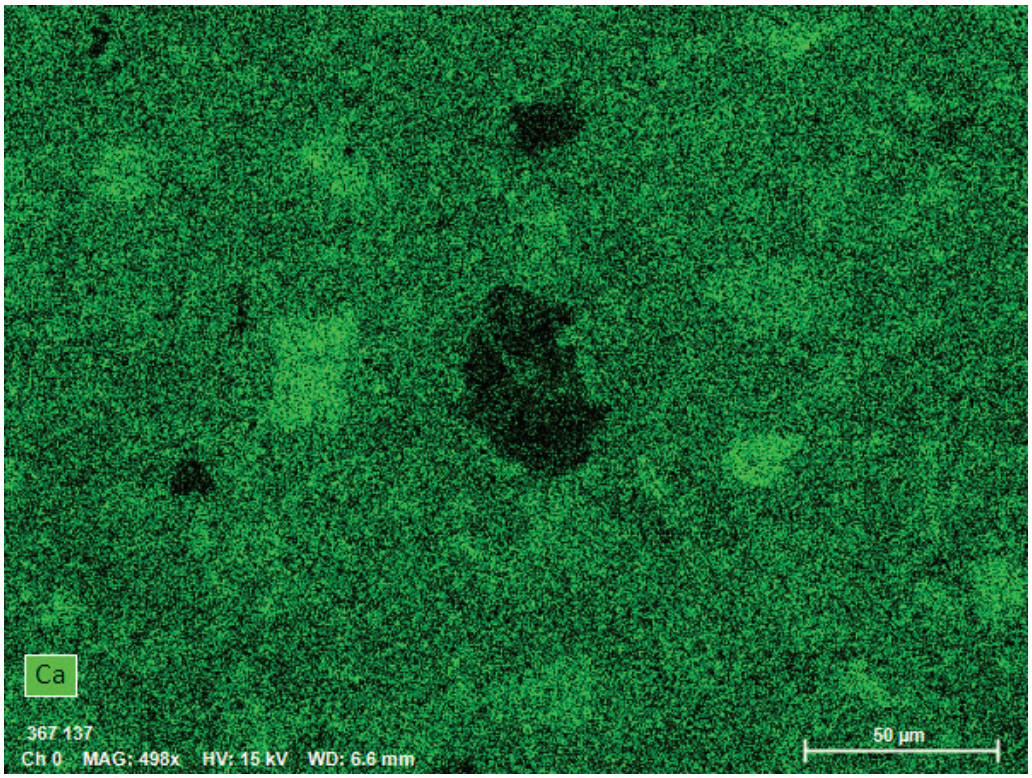

Figure B-7. EDS map of magnesium.

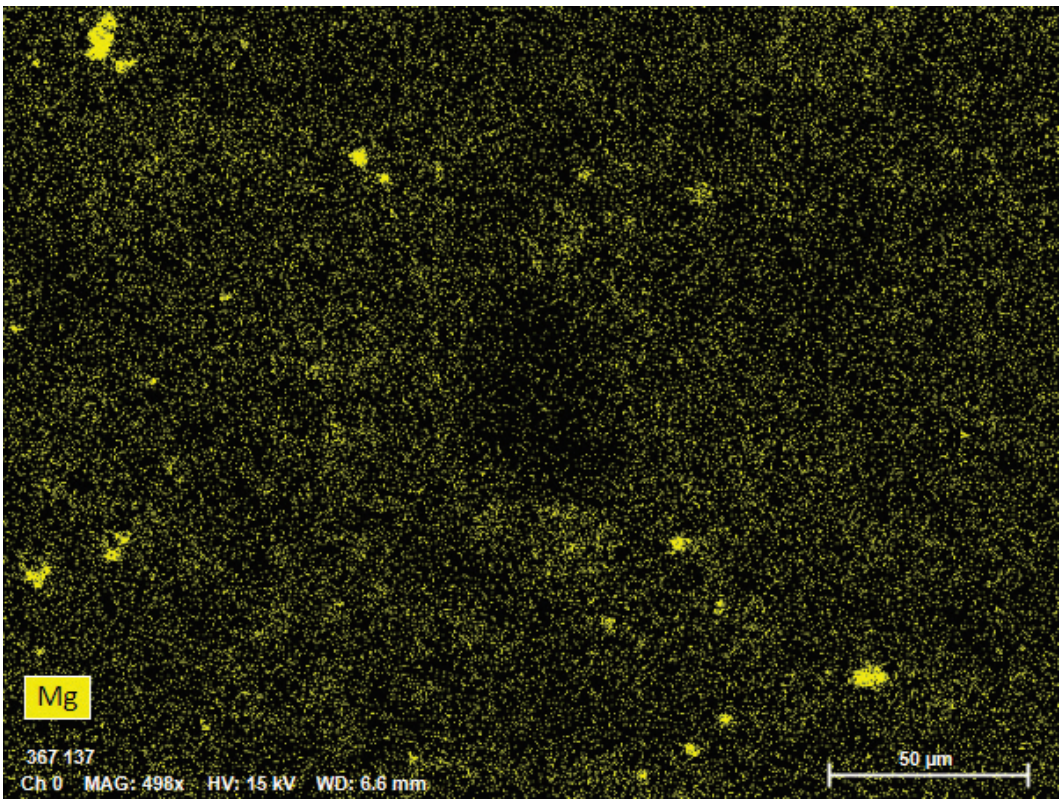

Abbreviations

ASTM	American Society for Testing and Materials
ATR	Attenuated total reflection
BW	Barite World
CGG	Commercial-grade graphene
CSH	Calcium silicate hydrate
EDS	Energy-dispersive x-ray spectroscopy
ERDC	Engineer Research and Development Center
FTIR	Fourier-transform infrared spectroscopy
FWHM	Full width at half maximum
GRM	Graphene-related materials
HRWRA	High-range water-reducing admixtures
LGG	Laboratory-generated graphene
SEM	Scanning electron microscope
TG	Turbo graphene
VCD	Voltage-high contrast detector
w/c	Water-to-cement ratio
w/w	Weight for weight
XPS	X-ray photoelectron spectroscopy
XRD	X-ray diffraction

REPORT DOCUMENTATION PAGE

Form Approved
OMB No. 0704-0188

1. REPORT DATE *(DD-MM-YYYY)*	2. REPORT TYPE	3. DATES COVERED *(From - To)*
December 2023	Final	FY21–FY22

4. TITLE AND SUBTITLE

Graphene in Cementitious Materials

5a. CONTRACT NUMBER

5b. GRANT NUMBER

5c. PROGRAM ELEMENT NUMBER
0603119A

6. AUTHOR(S)

Mine G. Ucak-Astarlioglu, Jedadiah F. Burroughs, Charles A. Weiss Jr., Kyle L. Klaus, Stephen L. Murrell, Samuel L. Craig, Jameson D. Shannon, Robert D. Moser, Kevin M. Wyss, and James M. Tour

5d. PROJECT NUMBER
505343

5e. TASK NUMBER
BO340

5f. WORK UNIT NUMBER

7. PERFORMING ORGANIZATION NAME(S) AND ADDRESS(ES)

See next page

8. PERFORMING ORGANIZATION REPORT NUMBER

ERDC/GSL TR-23-19

9. SPONSORING / MONITORING AGENCY NAME(S) AND ADDRESS(ES)

Office of the Assistant Secretary of the Army for Acquisition, Logistics, and Technology
Headquarters, US Army Corps of Engineers
441 G St. NW
Washington, DC 20314-1000

10. SPONSOR/MONITOR'S ACRONYM(S)

ASA(ALT)

11. SPONSOR/MONITOR'S REPORT NUMBER(S)

12. DISTRIBUTION / AVAILABILITY STATEMENT
Distribution Statement A. Approved for public release: distribution is unlimited.

13. SUPPLEMENTARY NOTES
Graphene Applications for Military Engineering

14. ABSTRACT

This project aims to determine the influence of laboratory-generated graphene (LGG) and commercial-grade graphene (CGG) on the chemical structure and compressive strength of graphene-cement mixtures. Determining the graphene-cement structure/processing/property relationships provides the most useful information for attaining the highest compressive strength. Graphene dose and particle size, speed of mixing, and dispersant agent were found to have important roles in graphene dispersion by affecting the adhesion forces between calcium silicate hydrate (CSH) gels and graphene surfaces that result in the enhanced strength of cement-graphene mixtures.

X-ray diffraction (XRD), Raman, and scanning electron microscope (SEM) analyses were used to determine chemical microstructure, and compression testing for mechanical properties characterization, respectively. Based on observed results both LGG and CGG graphene cement mixtures showed an increase in the compressive strength over 7-, 14-, and 28-day age curing periods. Preliminary dispersion studies were performed to determine the most effective surfactant for graphene dispersion.

Future studies will continue to research graphene—cement mortar and graphene—concrete composites using the most feasible graphene materials. These studies will prove invaluable for military programs, warfighter support, climate change, and civil works.

15. SUBJECT TERMS

Feasible graphene materials
Optimum graphene dispersion
Improving compressive strength
XPS
XRD
Raman
SEM/EDS analyses
Military construction
Warfighter support
Civil works infrastructure

16. SECURITY CLASSIFICATION OF:			17. LIMITATION OF ABSTRACT	18. NUMBER OF PAGES	19a. NAME OF RESPONSIBLE PERSON
a. REPORT	b. ABSTRACT	c. THIS PAGE			19b. TELEPHONE NUMBER *(include area code)*
Unclassified	Unclassified	Unclassified	SAR	64	

7. PERFORMING ORGANIZATION NAME(S) AND ADDRESS(ES)

US Army Engineer Research and Development Center (ERDC)
Geotechnical and Structures Laboratory (GSL)
3909 Halls Ferry Road
Vicksburg, MS 39180-6199

Rice University
NanoCarbon Center, MS-222
6100 Main St.
Houston, TX 77005